Study on a short pulse multiline CO_2 laser amplification system

February 1980

Yoshiyuki KAWAMURA

Preface

A CO_2 laser is one of the most feasible energy drivers which can be used for an inertial confinement fusion reactor because of its high energy conversion efficiency and high repetition rate. In this thesis, the studies on developing a high power CO_2 laser system are described, to which the author has contributed in the Institute of Laser Engineering of Osaka University.

Contents

Chapter 1 Introduction

1.1 CO_2 lasers as an energy driver for an inertial confinement fusion

For an inertial confinement fusion (ICF) by pellet implosion, where a large amount of energy must be injected into the fuel pellet before the fuel dissipated outwards, the energy drivers must satisfy the following conditions. (1) The output energies must be large ($\sim$100 kJ for Break-even, $\sim$1 MJ for reactor). (2) Their peak powers should be high ($\sim$100 TW). (3) The pulse duration must be as short as the implosion time of pellet. (4) A high S/N (signal to noise ratio) is required not to heat the fuel before the injection of the main laser pulse. (5) The focussability must be excellent to obtain high power density. (6) The transport efficiency from the driver to the pellet must be high. As to a practical ICF reactor, the following two conditions must be satisfied in addition to the above-mentioned conditions. (7) The conversion efficiency from the electric input energy to the laser output energy of the driver must be high. (8) High repetition rate can be obtained.

Several energy drivers have been developed, such as glass lasers, CO_2 lasers, relativistic electron beams, light ion beams, and heavy ion beams. From the view point of the focussability and transport, lasers have by far the best performance among them. Another advantage is that they can easily produce short pulses with desired pulse shape for the pellet implosion, because a high power laser system is constructed by the combination of an oscillator stage with

an amplifier stage. Because of these two advantages, lasers have been considered to be the best energy drivers for an inertial confinement fusion.

Glass lasers are the most advanced high power ones. Optical materials and components have been developed for the wavelength of the glass lasers. The Lawrence Livermore Laboratory has constructed a 10 kJ - 1 ns (nanosecond) laser system (Shiva), and a 100 kJ - 1 ns laser system (Nova) is under development. In the Institute of Laser Engineering (ILE) of Osaka University, a 20 kJ - 1 ns laser system (GekkoXII) is in course of construction and implosion experiments are being made by a 2 kJ - 1 ns laser system (Gekko IV). The glass lasers have several disadvantages in using in the practical ICF reactor. The efficiency (conversion efficiency from the electric input energy to the laser output energy) is low. High repetition rate can not be obtained due to the low cooling rate of the glass rods.

The CO_2 laser is the most feasible laser which can overcome these difficulties. Energy conversion efficiency of more than 10 % can be obtained because of their high pumping efficiency by optimized discharge through laser media. Repetition rate of more than 1 pps can be obtained. In the Los Alamos Scientific Laboratory, a 100 kJ - 1 ns CO_2 laser system (Antares) is under development, and a 10 kJ-1 ns laser system (Helios) has recently been used for implosion experiments. In ILE, a 10 kJ - 1 ns laser system (Lekko VIII) is under construction, and a 1 kJ - 1 ns laser system (Lekko II) is operating for implosion experiments and laser-plasma interaction experiments.

1.2 CO_2 laser fundamentals

Carbon dioxide is a linear symmetric molecule which has an axis of symmetry and a plane of symmetry perpendicular to the axis. There are three normal modes of vibration, ν_1, ν_2 and ν_3, as shown in Fig.1-1. For every mode of vibration, there exists a set of vibrational energy levels as shown in Fig.1-2. Among these low-lying vibrational levels, C.K.N. Patel found laser transitions from the (001) level to the (100) and (020) levels which are described by

$$CO_2(001) \rightarrow CO_2(100) + h\nu(10.4\ \mu m) \qquad 1\text{-}1$$

$$CO_2(001) \rightarrow CO_2(020) + h\nu(9.4\ \mu m) \qquad 1\text{-}2$$

For each vibrational state, there exists a set of rotational levels. The population N_j of the various rotational levels can be described by the Boltzmann distribution as

$$N_j \simeq N_t(hcB/kT)(2J+1)\exp[-BJ(J+1)hc/kT] \qquad 1\text{-}3$$

where N_t is the population density of total rotational levels, h is the Plank constant, c is the velocity of light, B is the rotational constant, k is the Boltzmann constant, T is the translational temperature of gas, and J is the rotational quantum number. Only odd rotational numbers are permitted for the upper laser levels and only even rotational numbers are allowed for the lower laser levels. Between these two rotational levels, laser transitions occur and only the transitions of $\Delta J = \pm 1$ can be allowed.

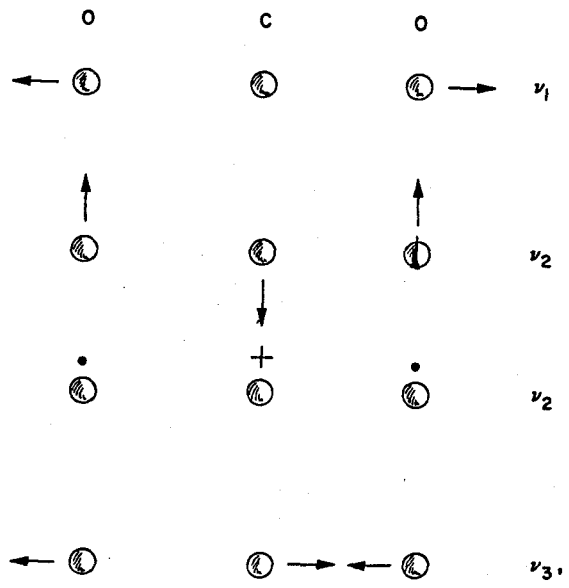

Fig.1-1. Normal vibration of CO_2 molecule:symmetric (ν_1), bent (ν_2), and asymmetric (ν_3) modes.

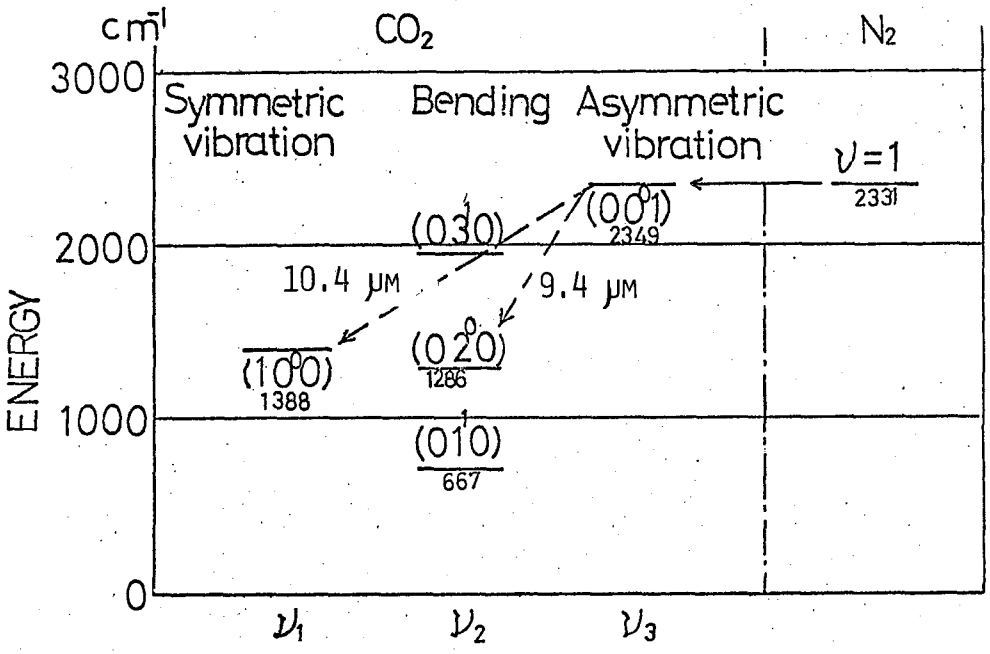

Fig.1-2. Vibrational levels of CO_2-N_2 system

Laser transitions with $\Delta J=1$ and $\Delta J=-1$ are named P branch and R branch respectively. Fig.1-3 gives a detailed transition diagram for laser transitions of both P and R branches of the 10.4 μm and 9.4 μm bands. The thermal distribution of the rotational levels in the (001) upper vibrational level for $B=0.38714\ cm^{-1}$ and T=400 K is shown in Fig.1-4. The J_{max} at which N_j has the maximum value is obtained from the equation 1-3 and is given by

$$J_{max} = \frac{1}{2}\left[(2kT/hcB)^{\frac{1}{2}}-1\right] \qquad 1\text{-}4$$

In an ordinary CO_2 laser in which the temperature of the laser medium is about 400 K, J_{max} is 19, so the P(20) line has the largest gain. The main feature of the CO_2 laser is that the quantum energy exsists in the upper vibrational level being distributed over several rotational levels, which affect the characteristics of the CO_2 laser oscillations and amplifications, especially in short pulse operation of ns.

Based upon consideration of optical energy storage, electrical pumping has been found to be the most efficient and scalable process. In electrically pumped CO_2 lasers, the upper levels are excited by inelastic electron-molecule collisions. The process is represented by

$$CO_2(000) + e(\varepsilon_k) \longrightarrow CO_2(\nu_1, \nu_2, \nu_3) \qquad 1\text{-}5$$

where (000) indicates the ground state and ε_k is the electron energy. The excitation rate of the various levels

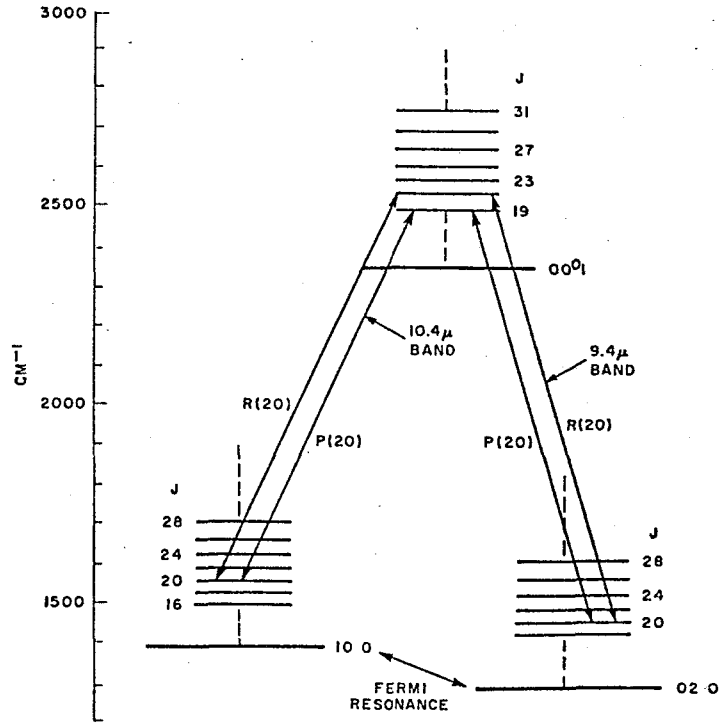

Fig.1- 3 A detailed laser transition diagram for the 001-100 and 001-020 bands, including rotational levels.

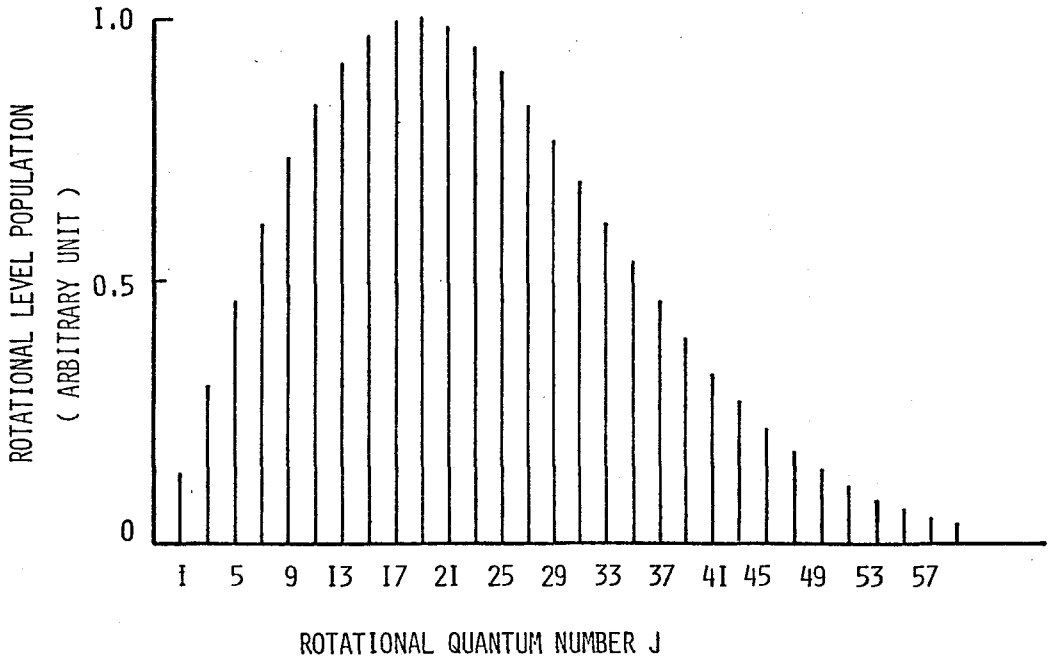

Fig.1-4 Thermal distribution of rotational level population in the 001 upper laser states.

is a strong function of electron energy, which in turn depends upon the ratio of discharge electric field to laser pressure, E/P.

1.3 High power CO_2 laser systems

In this section, a high power CO_2 laser system "Lekko-Ⅱ" is described, which has been developed and constructed in the CO_2 laser division of ILE. In general, a laser amplification system consists of three stages. The first stage is the oscillator stage, where the short pulses are produced. The second is the preamplifier stage. The third is the main amplifier stage, where the laser beam is saturation-amplified to extract the stored energy as much as possible. The "Lekko-Ⅱ" system is shown in Fig.1-5. A train of short pulses having a pulse width of $\sim$ 1 ns in the FWHM (full width at half maximum) is produced by a modelock oscillator, and one of them is sliced out by an electro-optic shutter. At the exit of the shutter, S/N of $\sim 10^4$ can be obtained. The energy and diameter of the laser pulse are $\sim$ 1 mJ and $\sim$ 0.8 cm respectively. It is amplified by Preamp.1 and Preamp.2. Both consist of several transversely excited atmospheric (TEA) CO_2 lasers, and the total length of the active gas is 300 cm. At the exit of Preamp.2, the energy and the beam diameter are $\sim$100 mJ and $\sim$2.5 cm respectively. The laser beam is expanded by a confocal mirror pair (U.G.-3) and an off-axial mirror pair (B.E.) to be 10 cm in diameter, and amplified by the final preamplifier (Amp.2) to be $\sim$ 5 J in energy. S/N decreases by saturation-amplification,

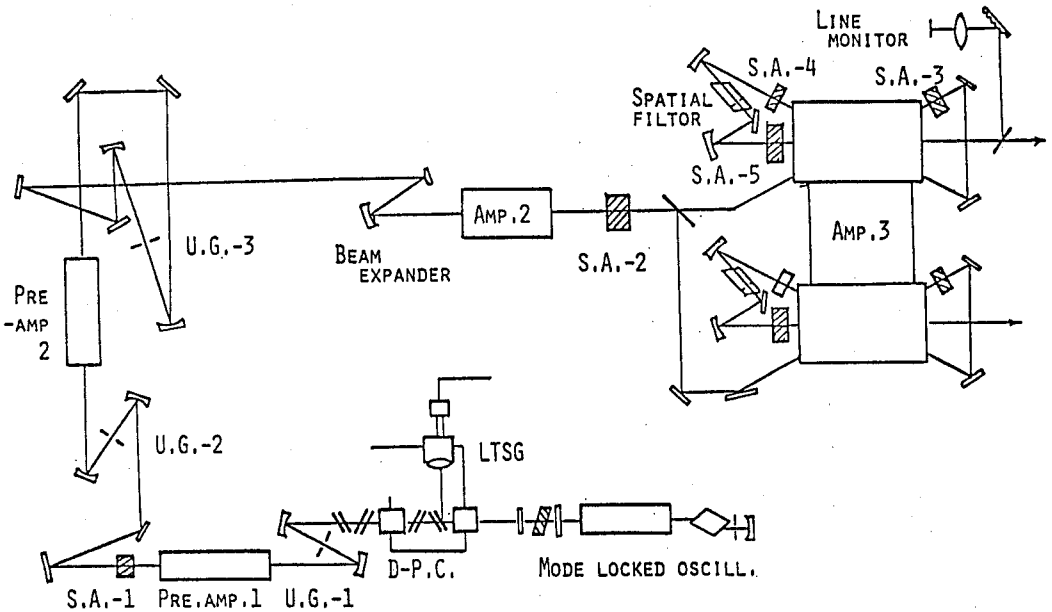

Fig.1-5. Schematic diagram of LEKKO-Ⅱ .

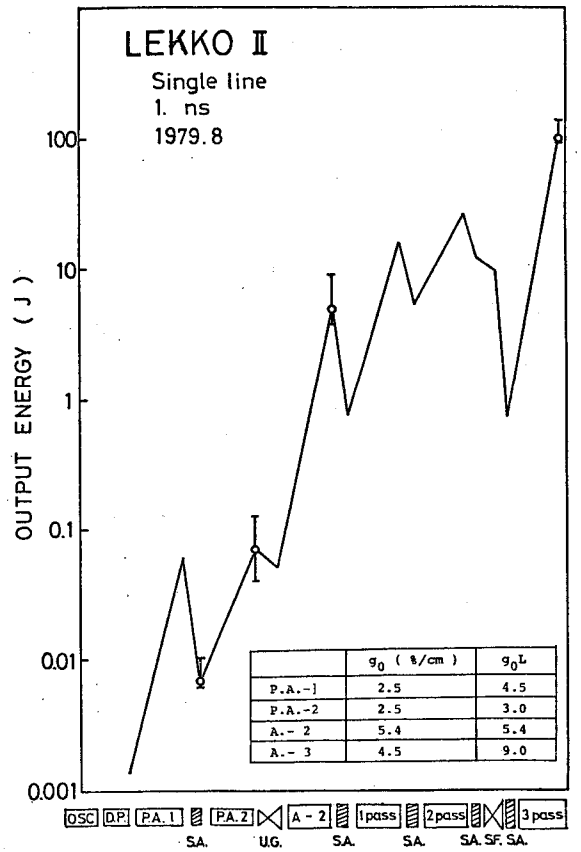

Fig.1-6. Operational performance of LEKKO-Ⅱ

therefore saturable absorber gas cells (S.A.-1 ∼ S.A.-5) are placed in the suitable places in the amplifier chain. The final amplifier is an electron beam controlled CO_2 laser amplifier having a three path optics to obtain saturation-amplifications. Beam diameter at the final path is 20 cm. The total gas pressure can be increased upto 2 atm. The final output energy of 200 J/beam having a pulse width of 1 ns was obtained, when the oscillation line was the P(20) line in the 10.4 μm band, the total gas pressure was 1.2 atm, and E/P was 6.25 kV/cm atm. For multiline amplification, the output energy of 400 J/beam can be expected.

Chapter 2 Study on an ultra short pulse multiline CO_2 laser oscillator

2.1 Introduction

In short pulse energy extraction from a CO_2 laser amplifier, multiline double-band oscillation and amplification are necessary in order to extract the stored energy efficiently from the amplifier. In this chapter, characteristics of multiline double-band oscillation using a gain-Q-switching TEA (transversely excited atmospheric) CO_2 laser oscillator and a modelock TEA CO_2 laser oscillator are described.

Several methods have been reported to obtain multiline double-band oscillations from a CO_2 laser oscillator at atmospheric pressure. Inter-cavity etalon,[1] high-gain oscillation systems,[2] inter-cavity gaseous absorber methods,[3,4] and double-cavity method using a grating,[5] have been studied. In this experiment, simultaneous oscillations up to nine lines were obtained by placing an etalon perpendicular to the optical axis of a gain-Q-switching[a)] TEA laser oscillator and varying the etalon thickness. Pulse widths of these gain-Q-switching multiline oscillations are 50$\sim$100 ns in the FWHM (full width at half maximum). In a high power short pulse CO_2 laser amplification system, short pulses are cut out from these gain-Q-switching pulses by an electro-

---

a) The CO_2 laser has a high small signal gain coefficient having a very fast risetime. Therefore, Q-switching oscillations can be obtained without using any optical components such as a bleachable dye cell and an electro-optic shutter.

optic gate. Recently, E.J. McLellan and J.F. Figueira[6] have succeeded in producing ultra short pulses as short as 90 ps in the FWHM.

Modelocking method is also a suitable way to generate a very short pulse with high power. Several works have been done in the area of generating a short pulse[7,8] and also in the area of making a multiline modelock pulse.[9,10] But the detailed characteristics of the multiline oscillation were not demonstrated especially for the modelock oscillation. In this chapter, the characteristics of the modelock multiline oscillation using an acousto-optic modulator and a TEA CO_2 laser are described.

2.2 Multiline gain -Q-switching oscillation

The experimental arrangement is shown in Fig.2-1. A TEA CO_2 laser was used. The length of the active gas was 600 mm. The curvature of the Au-coated mirror was 4000 mm, and the output mirror was Ge flat with polished and AR (anti-reflection) coated surfaces. The small signal gain was 3.4 %/cm in the 10.4 μm band P(20) line. Kodac Irtran NO.2 was used as an etalon to obtain multiline oscillations. The thickness, the refractive index, and the surface reflectivity were 3.15 mm, 2.19 (for the 10.4 μm band P(20) line), and 12 %, respectively.

Two methods were tested for changing the etalon thickness: (a) placing the etalon in the cavity perpendicularly to the optical axis and moving it to the direction perpendicular to that axis (the etalon had a slight taper, so the thickness along the optical axis was changed by this motion); (b)

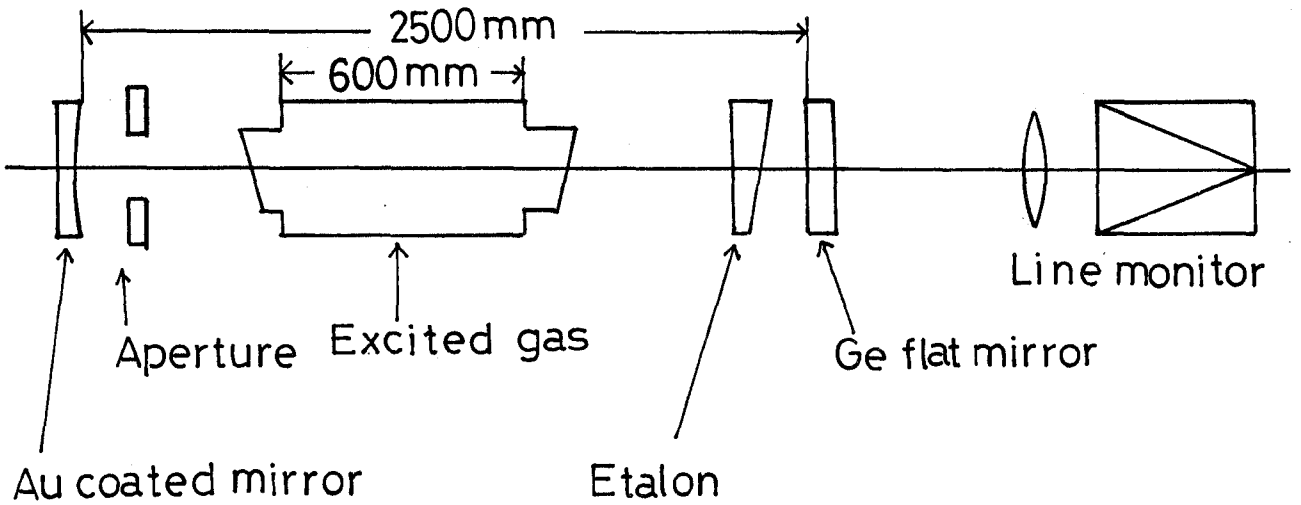

Fig.2-1. Experimental arrangement for multiline oscillation

placing the etalon in the cavity perpendicularly to the optical axis and tilting the etalon around an axis perpendicular to the optical axis. The number and the intensity of the laser oscillation lines were observed using a CO_2 spectrum analyzer (Laser Engineering Inc.). Method (a) was superior in reproducibility and stability. Seven oscillation lines P(14), P(16), P(18), P(20), R(14), R(16), and R(18) in the 10.4 μm band observed by the spectrum analyzer at the exit of the oscillator were compared with the theoretical etalon transmission curves. Very good agreements between the theory and the experimental results were obtained.

Fig.2-2 shows the variation of the oscillation lines as a function of the thickness of the etalon. Considering the transmission of each line for the etalon thickness between 3140 μm and 3160 μm, the 0 μm point on the upper horizontal scale was chosen to be 3144.5 μm. Fig.2-2 also shows that the selection of the oscillation lines can be explained by the theoretical transmission of the etalon. The effects of line competition were observed between the P(14) line and the R(12) line, and between the P(18) line and the R(16) line which had the same upper rotational levels (J=13 and J=17, respectively). When the P(14) line and the P(18) line appeared, the oscillations of the R(12) line and the R(16) line were suppressed.

2.3 Multiline modelock oscillation

There are two kinds of methods in modelocking,[11,12,13] namely passive modelocking and active modelocking. The former uses saturable absorbers such as a p-type germanium

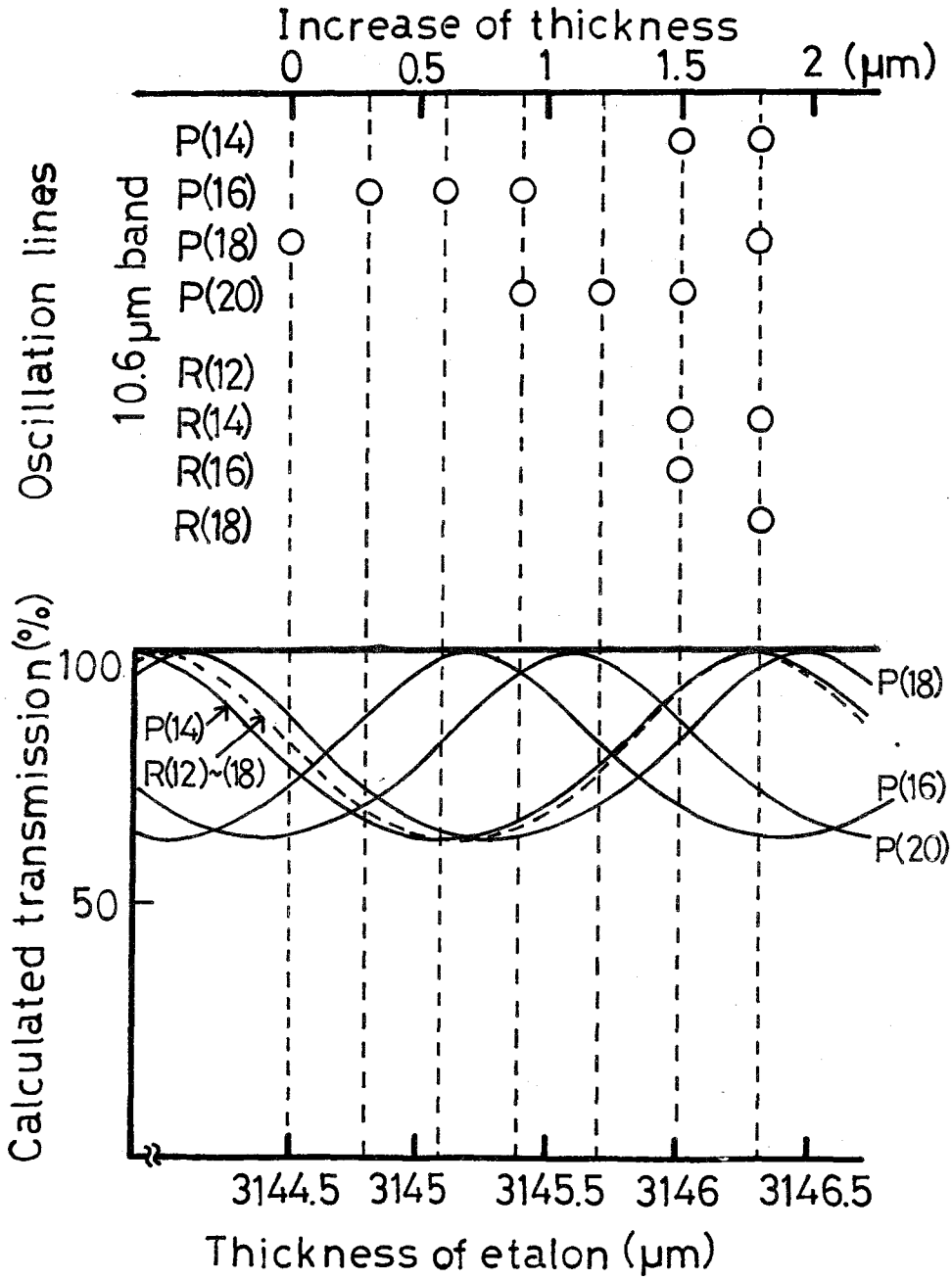

Fig.2-2. Oscillation lines observed and the calculated transmission of the etalon as a function of thickness (open circles signify the oscillation observed by the spectrum analyzer).

which was investigated aiming to get ultra short pulses from a high pressure CO_2 laser oscillator.[8] In the active modelocking, there are two kinds of methods. One is the acousto-optic modelocking method, where the diffraction loss induced by the acoustic standing wave in a germanium cristal is used to modulate a laser oscillation, and the other is the injection modelocking method where a laser oscillator is modulated by injecting an external cw (continuous wave) CO_2 laser beam into the laser cavity.

The characteristics of modelocking by an acousto-optical Ge modulator in the cavity had been investigated in detail to get reliable performance and smooth gaussian pulses of transform limit of gain media.[14] In this section, the characteristics of multiline modelock oscillation using a Brewster angle acousto-optic modulator are described.

The experimental setup is shown in Fig.2-3. A Brewster angle Ge modulator was used for modelocking, which was driven at the frequency of $\sim$20 MHz. The optical cavity was formed by a fully reflecting Au coated mirror with 5 m radius of curvature and an 89 % reflecting Ge flat mirror with the cavity length of 3.75 m. Active volume of a TEA CO_2 laser was 2cm $\times$ 2cm $\times$ 60cm. The discharge capacitor of 0.1 μF was charged to 30 kV. Mixing ratio of the laser gas was CO_2:N_2:He = 1:1:3. An NaCl plate was placed in the cavity as an etalon, whose parallelness and thickness were 15" and 5110 $\pm$ 5 μm respectively. It could be tilted around the axis perpendicular to the cavity axis as shown in Fig.2-3. The tilted angle θ, the angle between the cavity axis and the plane normal of the etalon, was chosen to be $\sim$

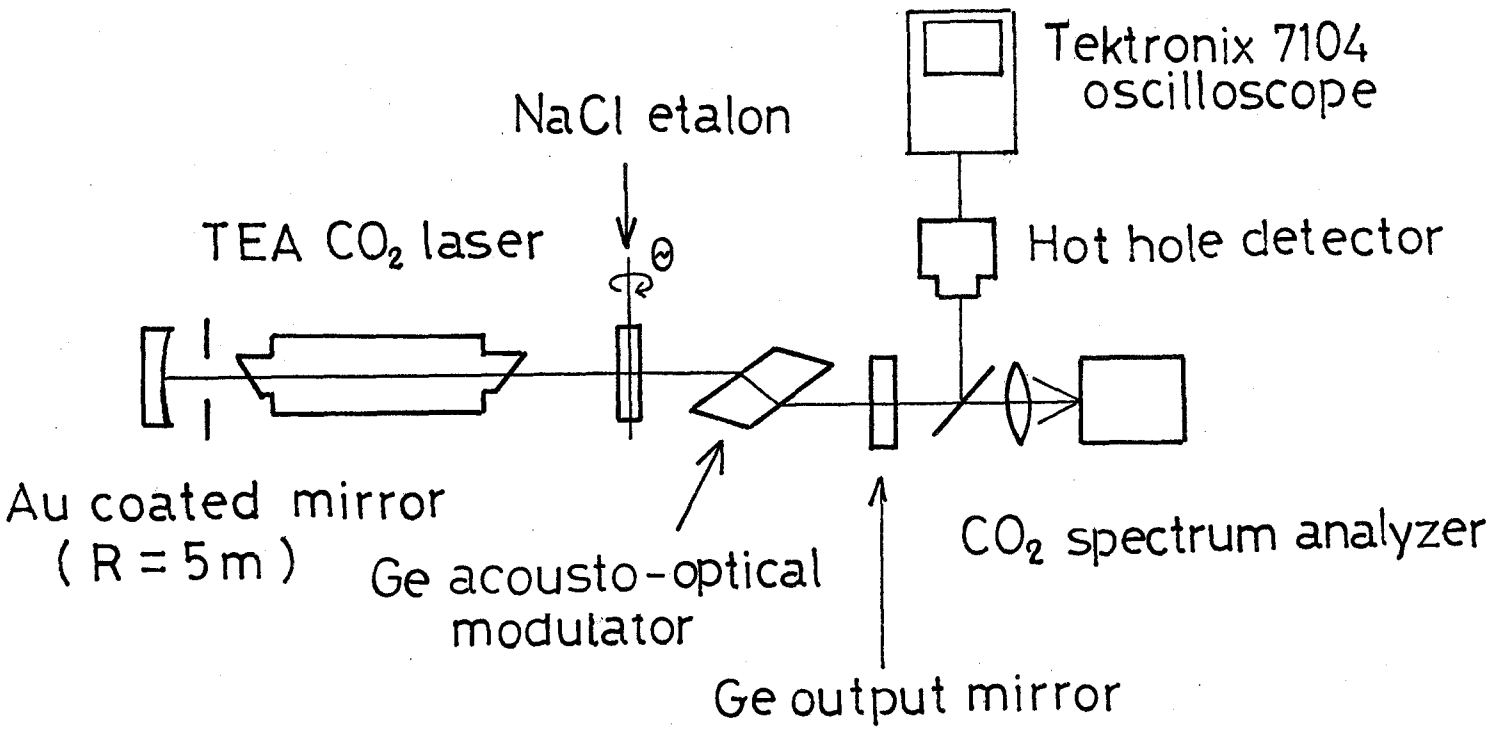

Fig.2-3. Experimental apparatus of the modelock multiline oscillation.

10°, $\sim 40^{\circ}$, and $\sim 50^{\circ}$ to vary the finesse of the etalon. The oscillation spectrum was measured by an Opt. Eng. CO_2 laser Spectrum Analyzer. The wave form was measured by a Rofin's hot hole detector (rise-time : 200 ps) connected to a 1 GHz oscilloscope (Tektronix 7104). The risetime of the detection system can be estimated to be $\sim$400 ps. The ambient temperature was kept to be $20 \pm 0.5^{\circ}C$.

Oscillation characteristics for $\theta \simeq 10^{\circ}$, $\theta \simeq 40^{\circ}$, and $\theta \simeq 50^{\circ}$ are shown in Fig.2-4, Fig.2-5, and Fig. 2-6 respectively. Open circles denote the operations of the gain-Q-switching oscillations obtained without operating the acousto-optic modulator. Black circles denote the operations of modelock oscillations. Both showed the same oscillation characteristics for each tilted angle of the etalon. For the oscillation lines of the P branch, the P(20) line has the widest angular range of oscillation and the P(14) line has the narrowest. The angular ranges where more than 3 simultaneous oscillations could be obtained were $\sim 0.04^{\circ}$, $\sim 0.021^{\circ}$, and $\sim 0.007^{\circ}$ for $\theta \simeq 10^{\circ}$, $\theta \simeq 40^{\circ}$, and $\theta \simeq 50^{\circ}$ respectively. They decreased as the finesse of the etalon increased.

In this section, normalized effective cavity gain $G(J,\theta)$ including the transmission of the etalon was introduced, to explain the multiline oscillation characteristics, which is given by

$$G(J,\theta) = T(J,\theta)\exp\{[g(J)-g(19)]\cdot L\} \qquad 2\text{-}1$$

where $T(J,\theta)$ is the transmission of the etalon for the rotational quantum number J at the etalon tilted angle θ.

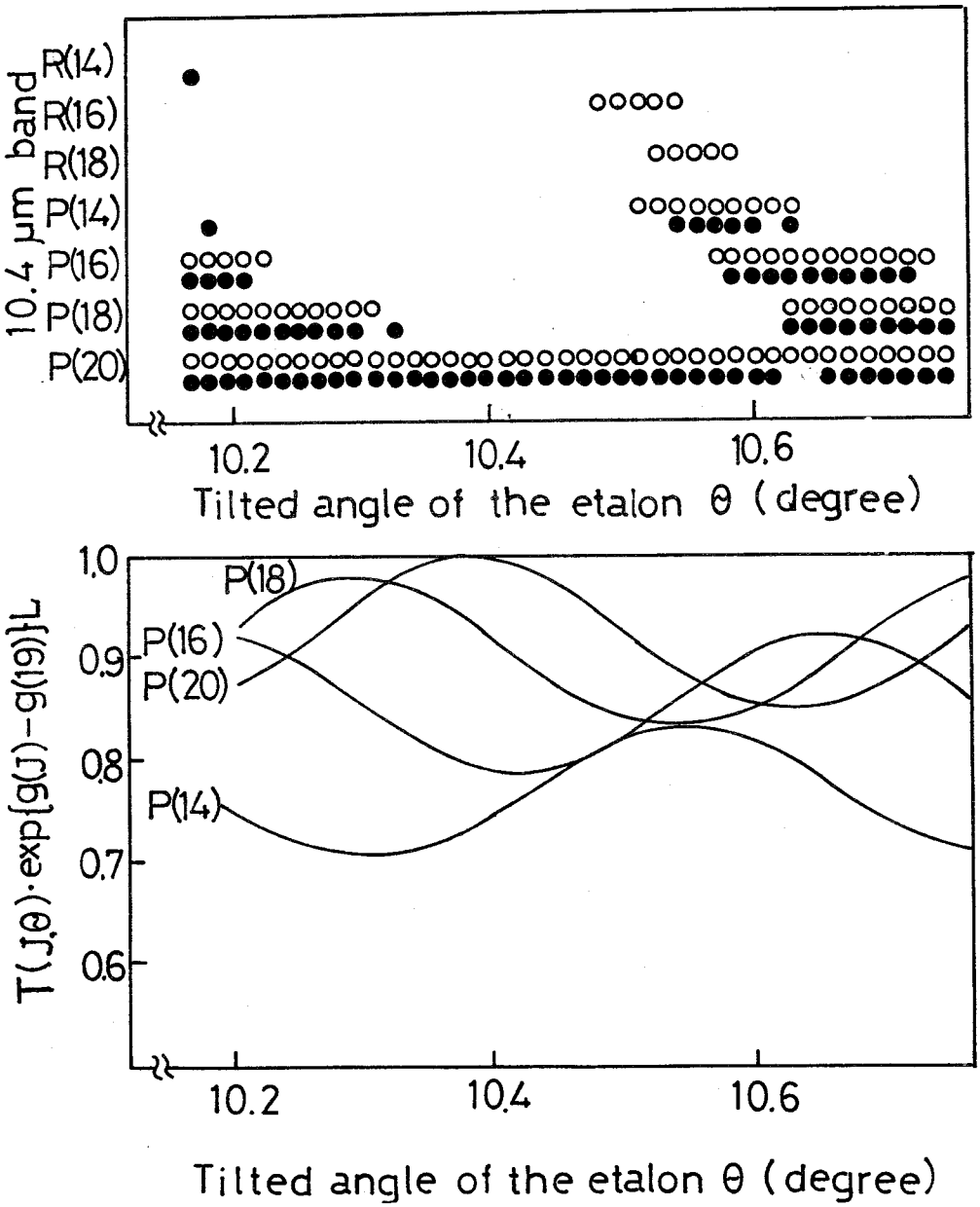

Fig.2-4. Multiline oscillation characteristics and the effective cavity gain for each line ($\theta = 10^{o}$). (Open circles and black circles denote gain-Q-switching oscillations and modelock oscillations respectively.)

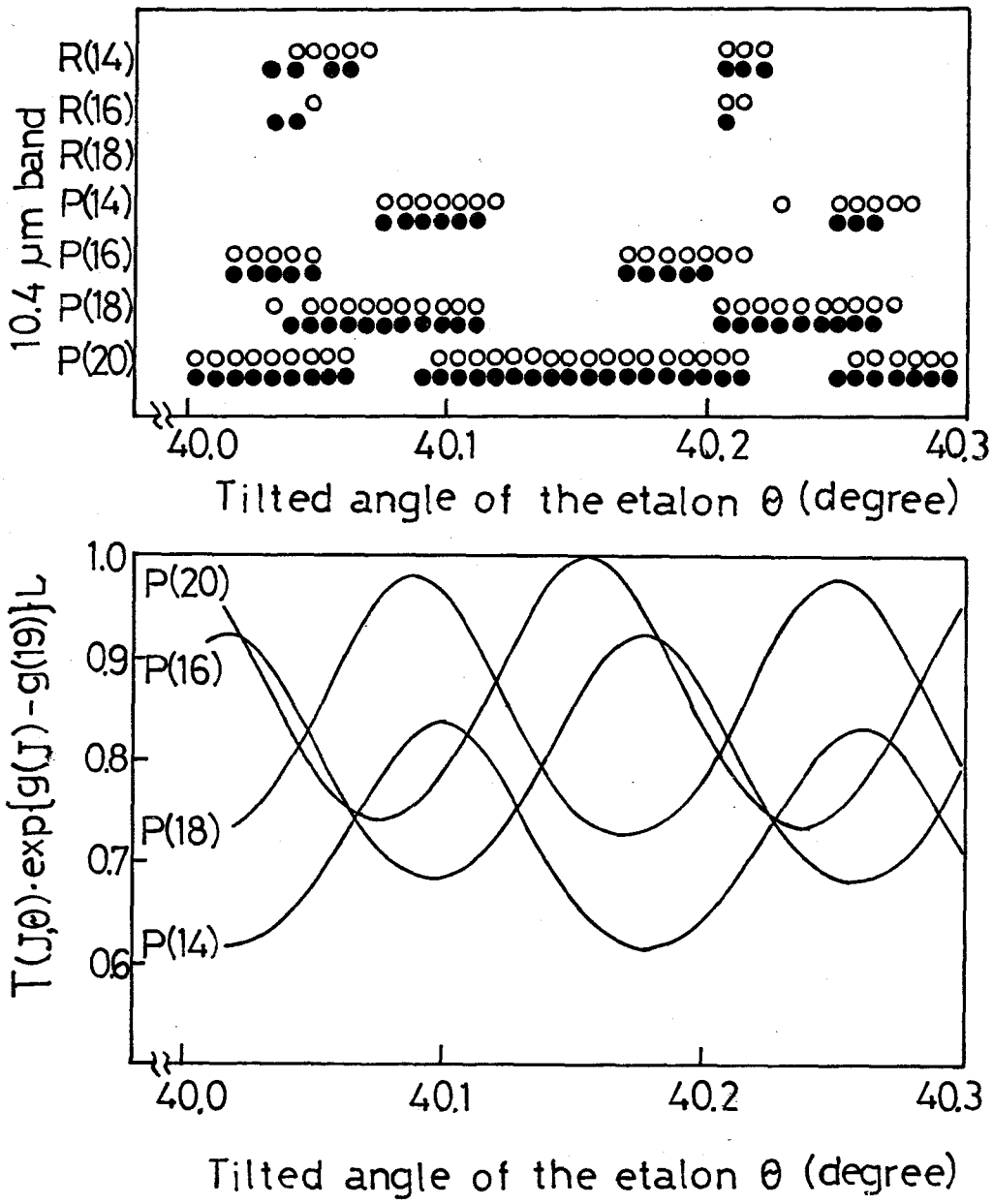

Fig.2-5. Multiline oscillation characteristics and the effective cavity gain for each line (θ = 40°). (Open circles and black circles denote gain-Q-switching oscillations and modelock oscillations respectively.)

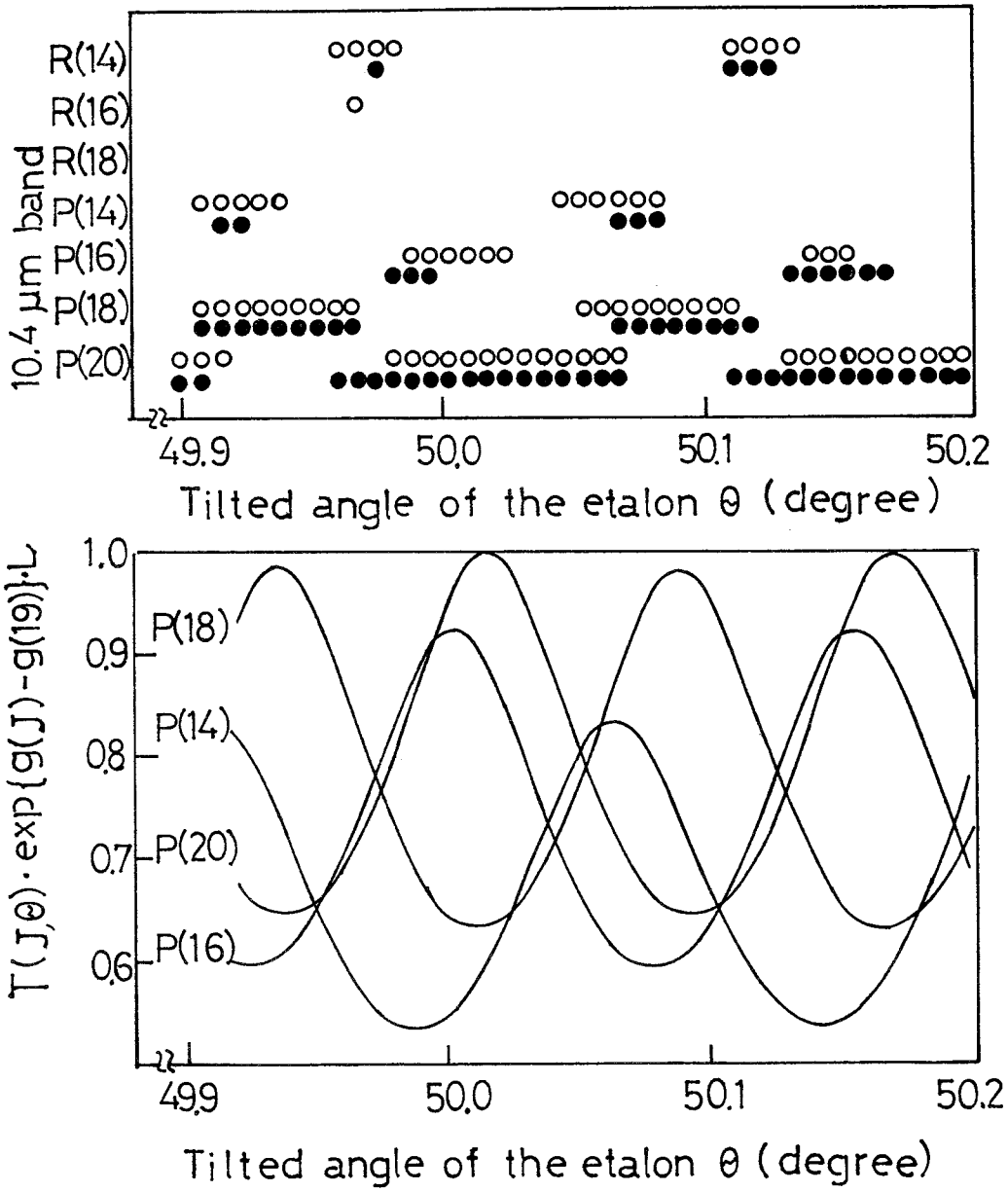

Fig.2-6. Multiline oscillation characteristics and the effective cavity gain for each line (θ = 50°). (Open circles and black circles denote gain-Q-switching oscillations and modelock oscillations respectively.)

g(J) is the small signal gain coefficient for the line of the rotational quantum number J. L is the active gas medium length. Without inserting the etalon in the cavity, the oscillation occurred at the P(20) line, which had the highest small signal gain over all the rotational lines. It was measured to be 3 %/cm by another experiment. The effective cavity gain $G(J, \theta)$ for several rotational lines is shown on the lower half in Fig.2-4, Fig.2-5,and Fig.2-6 as a function of the tilted angle θ. The oscillation occurred simultaneously when $G(J,\theta)$ for each line became approximately the same value.

Stability and reproducibility of the modelock oscillation were measured at $\theta = 50.067^{\circ}$ where the angular range of the multiline oscillation was the narrowest. Oscillation lines were the P(20), P(18), and P(14) lines in the 10.4 μm band. For at least 2 hours, perfect reproducibility of modelock multiline oscillations was obtained.

The pulse width τ_p(FWHM) and the risetime τ_r(10% to 90%) were measured by a Tektronix 7104 oscilloscope and a Rofin's hot hole detector. The averaged pulse width of 890± 70 (standard deviation) ps was obtained for the single line operation.

A typical waveform of the single line modelock oscillation is shown in Fig.2-7. According to the theory for a steady state AM (amplitude modulation) modelocking of a homogeneously broadened laser developed by D.J. Kuizenga and A.E. Siegman[15], a minimum pulse width τ_{pt} obtained by such a laser is given by

$$\tau_{pt} = \frac{\sqrt{2\ \ln 2}}{\pi}\ \frac{g^{1/4}}{\theta_m^{1/2}}\left(\frac{1}{f_m \cdot \Delta f}\right)^{1/2} \qquad 2\text{-}2$$

where f_m and Δf are the modulation frequency and the band width the gain spectrum respectively. g and θ_m are the saturation round-trip amplitude gain of the laser medium and the depth of modulation, and determined by $g=\ln(1/R)$ and $T(t)=\cos(\theta_m \sin 2\pi f_m t)$ respectively.

R: effective(power) reflection of a mirror including all cavity losses.

T(t): amplitude transmission through the modulator.

Δf was calculated to be 3.64×10^9 Hz for the laser gas mixture of $CO_2:N_2:He = 1:1:3$.[16] θ_m and g are calculated to be 1.16 and 0.223 respectively using T(t)=0.4 and R=0.8. Substituting $\theta_m=1.16$, $g=0.223$, $f_m=2.0 \times 10^7$, and $f=3.64 \times 10^9$ into the equation 2-2, τ_{pt} becomes 887 ps which coincides with the experimental result. For the multiline oscillation, single envelope modelock pulses were obtained, whose τ_p and τ_r were 980 ± 40 ps and 660 ± 50 ps respectively. The minimum pulse width of 730 ps was obtained as an exception, which was by far the narrowest among the others and did not have a gaussian shape as shown in Fig 2-8. Such pulse shape is considered to appear when the modulation frequency differs slightly from the optical resonator frquency.

In conclusion, it has been demonstrated that (1) a stable modelock multiline operation of a TEA CO_2 laser was obtained, (2) output spectrum was controlled by an etalon and the oscillation characteristics were explained by introducing the effective cavity gain, and (3) waveforms of the modelock oscillation were measured by a fast response detection system. It was also shown that using an active modelock oscillator of a TEA CO_2 laser, averaged pulse width

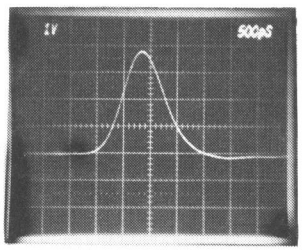

Fig.2-7. A typical waveform of the single line modelock oscillation.

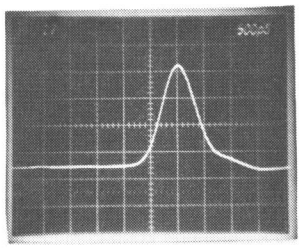

Fig.2-8. The waveform of the single line oscillation laser pulse with the pulse width of 730 ps in the FWHM.

of 890 ps was obtained which coincided with the theoretical estimation assuming a steady state AM modelock operation of a homogeneously broadened laser.

2.4 Summary

In this chapter, characteristics of multiline oscillation using inter-cavity etalon were described for gain-Q-switching oscillations and acousto-optic modelock oscillations. Multiline oscillation characteristics for modelock oscillations were explained perfectly by using the total cavity gain including both the loss of the inter-cavity etalon and the gain of the active medium, as well as for gain-Q-switching oscillations. It was shown that stable modelock multiline oscillations could be obtained for long time. It was shown that subnanosecond pulses could be obtained for an acousto-optic modelocking of a TEA CO_2 laser.

Referances

1). M. Piltch, Opt. Commun. 7, 397 (1973).

2). M.C. Richardson, Opt. Commun. 10, 302 (1974).

3). G.T. Schappert and J.F. Figueira, Opt. Commun. 13, 104 (1975).

4). M. Matoba, Annual Progress Report of Institute of Laser Engineering, Osaka University, 1976, P.42 (unpublished)

5). M. Keller, M. Matoba, S.Nakai, and C. Yamanaka, Jpn. J. Appl. Phys. 14, 423 (1975).

6). E.J. McLellan and J.F. Figueira, Rev. Sci. Instrum. 50, 1213 (1979).

7). P.B. Corkum, A.J. Alcock, D.F. Rollin, and H.D. Morrison,

Appl. Phys. Lett. 32, 27 (1978).

8). H. Daido, T. Koide, M.Matoba, S. Nakai, and C. Yamanaka, J. J. Appl. Phys. 48, 424 (1979).

9). M.C. Richardson, Appl. Phys. Lett. 25, 31 (1974).

10). T. Sakane, Opt. Commun. 12, 21 (1974).

11). A.F. Gibson, et al., Appl. Phys. Lett. 18, 546 (1971).

12). R. Fortin, et al., Appl. Phys. Lett. 51, 414 (1973).

13). A.F. Gibson, et al., Appl. Phys. Lett. 24, 306 (1974).

14). Y. Kawamura, M. Matoba, S. Nakai, and C. Yamanaka, The Transaction of The Institute of Electrical Engineers of Japan, Vol 99-C, 251 (1979).

15). D.J. Kuizinger and A.E. Siegman, J. Quant. Elect. 6, 694 (1970).

16). R.L. Abrams, Appl. Phys. Lett. 25, 609 (1974).

Chaper 3. Study on an injection multiline oscillation

3.1 Introduction

Recently, the technique of pulse shaping has been developed and it has become possible to slice a single pulse having a duration of subnanosecond and a risetime of about a hundred picoseconds from a gain-Q-switching TEA CO_2 laser.[1] Especially in the aspect of a risetime, it exceeds the modelock oscillation using a TEA CO_2 laser whose risetime is limited by a frequency bandwidth of the laser medium. The pulses generated by gain-Q-switching oscillation of a TEA CO_2 laser generally exhibit a sharply spiked substructure produced by beating between a number of simultaneously oscillating longitudinal cavity modes. Mode selection or frequency control of oscillation is required to get smooth output pulses from which ns pulses are sliced out by a pulse shaping system.

The line control of a multiline oscillation is also required to the oscillator in a high power CO_2 laser system to improve the system efficiency in ns pulse amplification. In the previous chapter, the multiline oscillation characteristics of a gain-Q-switching TEA CO_2 laser using an etalon plate were described. An injection technique[2] is one of the feasible methods to obtain desired multiline oscillations and to control the oscillation mode simultaneously with high stability or reproducibility of operation.

Injection techniques, where a low power cw (continuous wave) injection signal can control a high power pulsed oscillator by injecting it into the resonator of the pulsed

oscillator during excitation, have been studied in the area of microwave resonators.[2] In the area of TEA CO_2 laser oscillators, several works have been done to force its longitudinal mode to that of the injection cw CO_2 laser (frequency locking) or to force the rotational transition line to that of the injection laser (line locking). J.L. Lachambre, et al.[3] showed that the frequency-locking zone, where the oscillation frequency of a high power TEA CO_2 laser could be locked to that of a master injection cw CO_2 laser, could not be found, even though they used the experimental apparatus having 3 MHz resolution which corresponds to the detuning angle of 0.03π. J.R. Izatt, et al.[4] showed that single-mode TEA-CO_2 laser pulses could be produced on a large number of lines in the P and R branches of both laser bands by injecting a few watts of cw CO_2 laser power, and simultaneous single-mode pulses on the P(18) and P(20) lines of the 10.4 μm band could be also produced by operating cw laser beams on both lines simultaneously. In their experiments, no length stabilization and frequency matching of the two resonators were required, which was expected to be necessary by the experimental result obtained by J.L. Lanchamber, et al. B.Gellert, et al.[5] showed the polarization, as well as laser oscillation lines, could be forced by a master cw injection signal. Also in their experiments, length stabilization or frequency matching was not required.

In this chapter, injection oscillation characteristics for several rotational transitions are described as a function of an injection laser power level and a detuning angle between the cw injection oscillator and a TEA CO_2

laser oscillator. A power spectrum analyzer was developed to measure energy fraction of each line in multiline operations.

3.2 Experiment and discussion

The experimental apparatus is shown in Fig.3-1. The master oscillator was a line-tunable cw CO_2 laser (NEC GLG 2048) with a cavity length of $\sim$1.3 m delivering TEM_{oo} output of several hundreds milliwatts in single longitudinal mode into the TEA laser. The direction of polarization of the master oscillator and the TEA oscillator were set to be the same. The injected cw laser power was measured behind an aperture A. The optical cavity of the TEA laser was formed by a fully reflecting Au coated mirror with 6 m radius of curvature and a 79% reflecting Ge flat mirror with cavity length of 3.5 m. The discharge tube was 60 cm in length, and had NaCl windows mounted at Brewster's angle. Two NaCl plates were placed in the cavity. One was for injecting the CW CO_2 laser power into the TEA CO_2 laser cavity, and the other was for shifting the longitudinal mode by changing the tilted angle. Both were slightly wedged to quench etalon effect. The latter was tilted around Brewster's angle not to cause optical loss. Aperture B just in front of the Au coated mirror was 9 mm in diameter and was used as a transverse mode selector. Oscillation waveforms of the TEA CO_2 laser were measured by a photon drag detector and a Tektronix 7904 oscilloscope. Optical Engineering Spectrum Analyzer was modified to measure energy fraction of each line of multiline oscillation. Wavelength display screen of it was replaced by the array of small calorimeters which

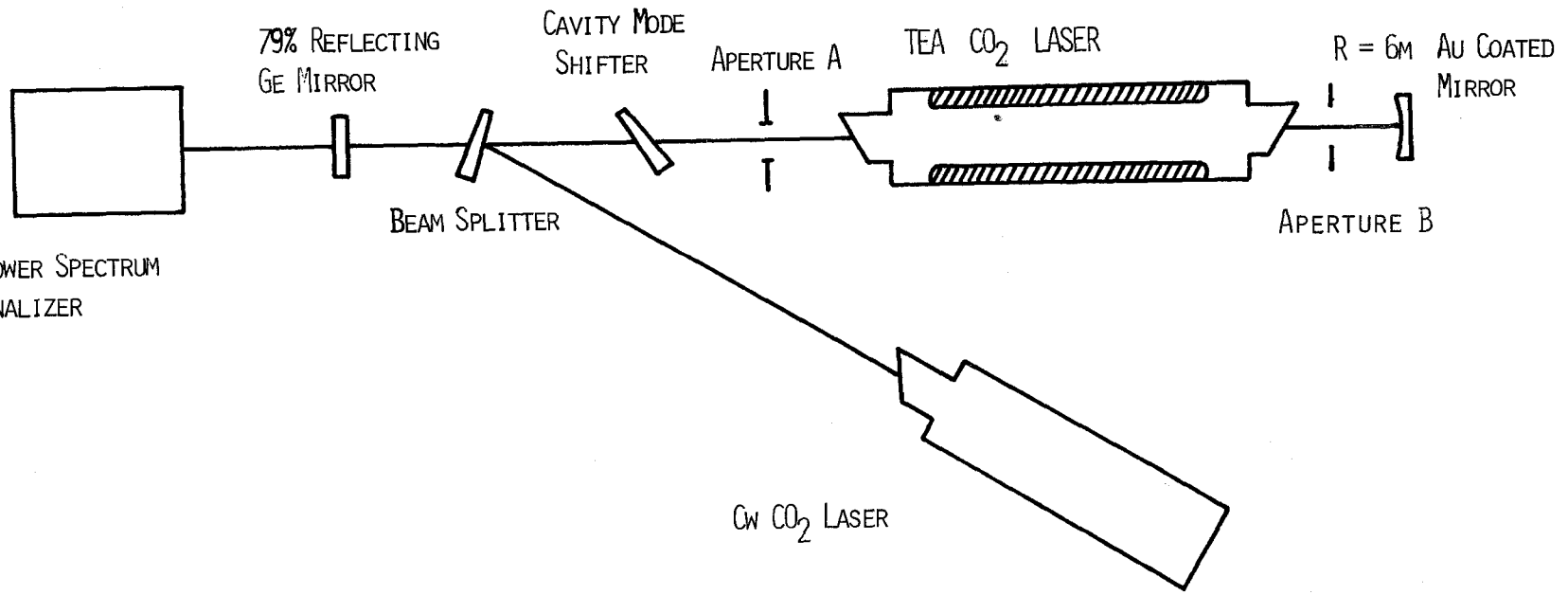

Fig.3-1. Experimental apparatus used for the injection line forcing.

were composed of Al_2O_3 coated Al block and thermo-couples, and the position of each calorimeter was adjusted on the focussing position of the different rotational transition lines.

Fig.3-2 (a) shows a typical multimode pulse produced by a free running TEA CO_2 laser which oscillated at the P(20) line in the 10.4 μm band. The spikes produced by beating of different cavity modes are separated by the round-trip time of about 23 ns. Fig.3-2 (b) shows a smoothed laser pulse obtained by injecting a low power cw CO_2 laser beam of the master oscillator, which was tuned at the P(20) line in the 10.4 μm band. With the injection laser power of $\sim$50 mW, the modulations have disappeared completely. The alignment was not critical for this experiment.

To measure line forcing characteristics of the injection laser system, the master oscillator was tuned to various lines in the 10.4 μm and 9.4 μm bands. Injection laser power was varied from $\sim$1 mW to $\sim$500 mW to know the threshold value for the initiation of injection line forcing. The experimental results are shown in Fig.3-3 and Fig.3-4. The fraction of the forced oscillation energy by the master oscillator in the total oscillation energy is shown as a function of injected cw laser power. For example, in Fig.3-3, at the injection power of 20 mW the energy fraction of the forced oscillation by a master oscillator at the P(22) line in the 9.4 μm band was 25% and the rest was the P(20) line in the 10.4 μm band. For all lines, injection line forcing effect showed qualitatively the same characteristics. Injection line forcing effects had the threshold power of

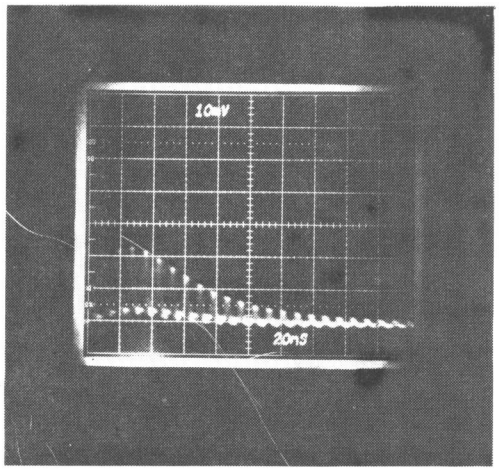

(a)

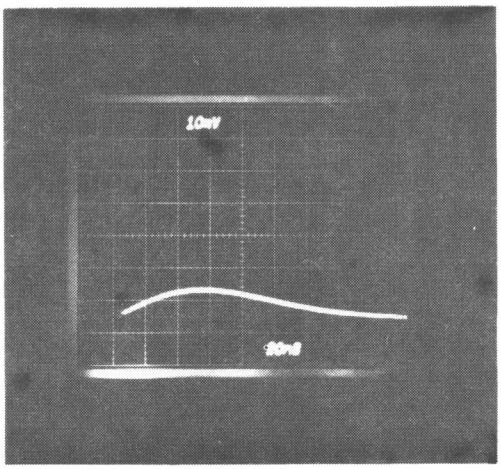

(b)

Fig.3-2. Smoothing effect of the injection technique. (The upper trace represents a free running of a TEA CO_2 laser. The lower trace represents a smoothed laser output waveform obtained by injecting cw CO_2 laser beam.)

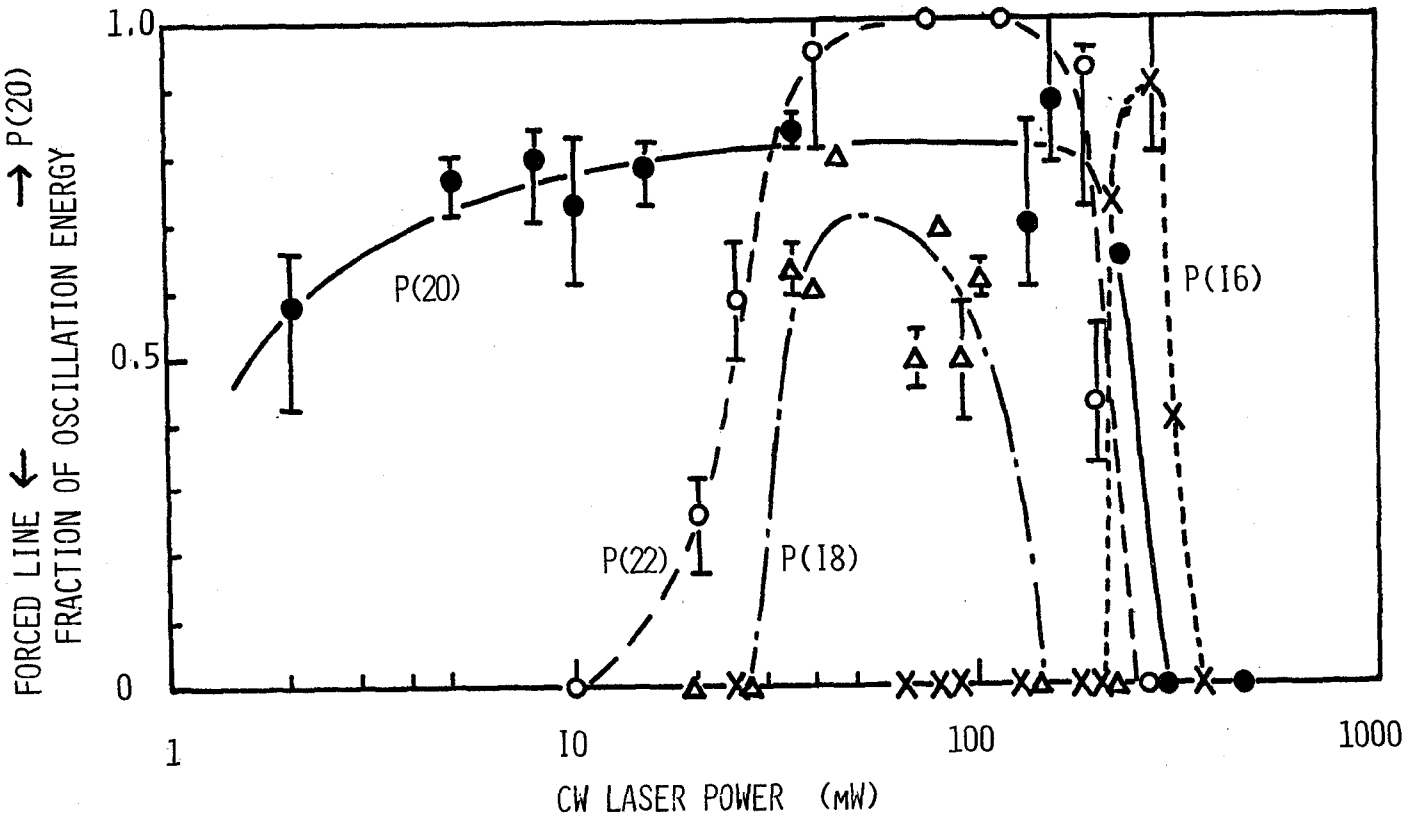

Fig.3-3. Fraction of line forced oscillation energy as a function of the injection cw CO_2 laser power of several lines in the 9.4 μm band.

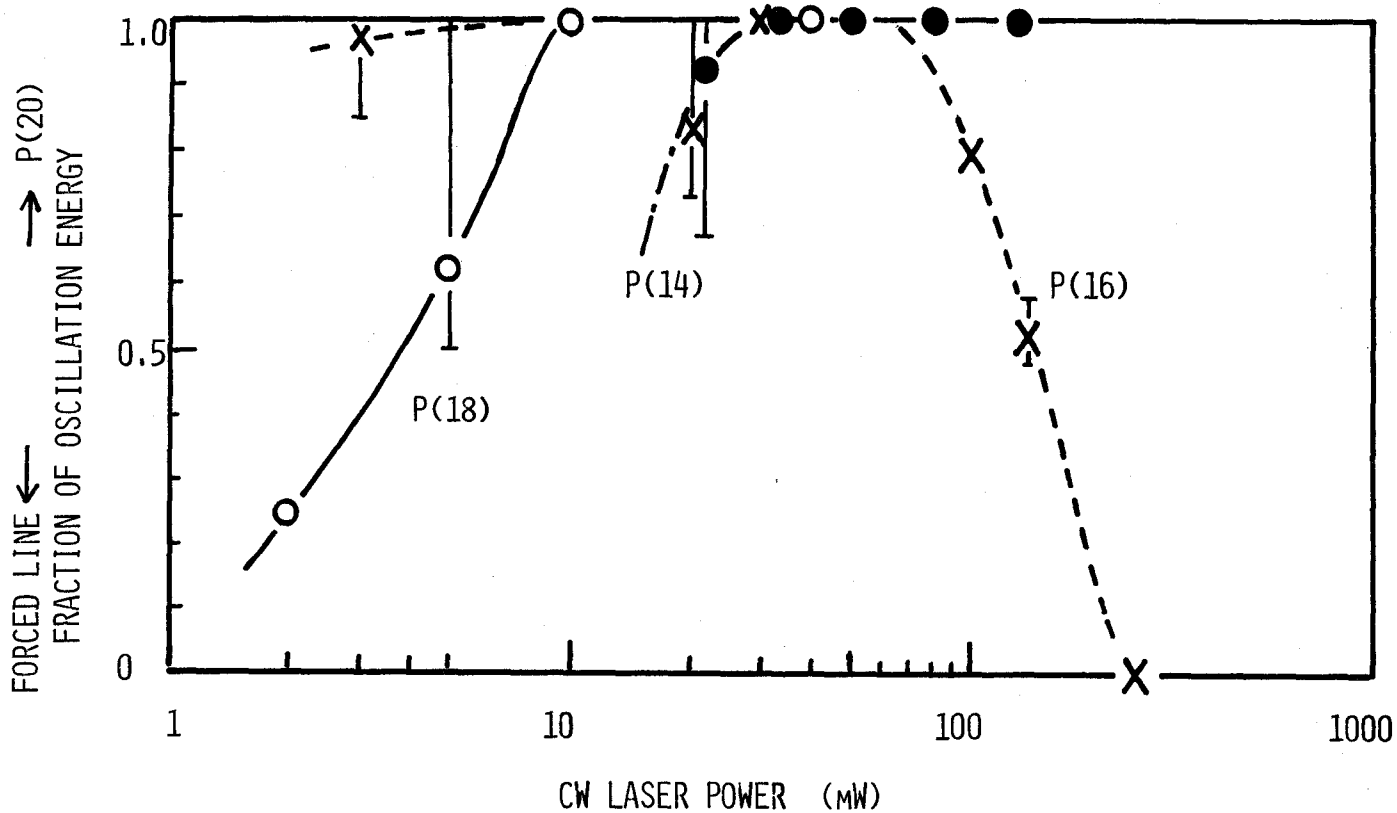

Fig.3-4. Fraction of line forced oscillation energy as a function of the injection cw CO_2 laser power of several lines in the 10.4 μm band.

the injection cw laser, and too much injection power quenched the line forcing effect. The threshold power of the injection laser for line forcing could be explained qualitatively, for example considering the small signal gain coefficient for each line. For quantitative discussions of these thresholds, more detailed experiments are required and will be discussed later.

Fig.3-5 (A)$\sim$ (D) show the waveforms of the injection line forced oscillations for various injection power levels. Fig.3-5 (a) shows the waveform of a free running oscillation at the P(20) line in the 10.4 μm band, which was obtained without injection of the cw laser. Many spikes caused by beating between different longitudinal modes are observed. By injecting cw laser power of $\lesssim$ 5 mW, the height of the spikes in the main pulse decreased, while those in the second pulse following the main pulse, did not decrease [see Fig.3-5(B)]. Considering the variation of the energy fraction of oscillation lines due to injection and the change of oscillation waveforms, spikes are considered to be the free running oscillation of the P(20) line in the 10.4 μm band and the low frequency components in the main pulse are considered to be the line forced oscillation of the P(16) line in the 10.4 μm band. For the injection power level of $\lesssim$ 10 mW, the spikes in the main pulse disappeared, while those in the second pulse still remained [see Fig.3-5(C)]. This experimental result shows that the injection effect to the main pulse induced by a gain-Q-switching oscillation is stronger than that to the second pulse induced by the re-excitation of the (001) vibrational level by the

resonanse transfer between the (001) level of CO_2 molecules and the first vibrational level of N_2 molecules. For the injection power of $\sim$30 mW, spikes in the second pulse disappeared and the oscillation line of the TEA laser was completely locked at the P(16) line in the 10.4 μm band [see Fig.3-5(D)].

The threshold power of injection for line forcing effects could be qualitatively explained by the small signal gain of each line. For quantitative explanation, detuning angles between the longitudinal modes of the cw laser and that of the TEA laser were introduced. The detuning angle was defined by the difference between the frequency of the longitudinal mode of the cw CO_2 laser and that of one of the longitudinal modes of the TEA CO_2 laser which is the nearest to the former. Where, the space of the longitudinal modes of the TEA CO_2 laser was chosen to be 2π. The thresholds were measured as a function of the detuning angle. As the measurement of the absolute detuning angle was difficult. Injection characteristics were measured for a certain detuning angle θ_0, $\theta_0+0.35\pi$, $\theta_0+0.37\pi$, and $\theta_0+0.70\pi$. The detuning angle was set with an accuracy of $\pm$ 0.1 π by changing the tilted angle of the NaCl plate. The experimental results are shown in Fig.3-6. The threshold injection powers for initiation of the line forcing are shown in Fig.3-7 as a function of the relative detuning angle. Here, θ_0 is assumed to be 0, because the threshold power has the minimum value at this angle. For the detuning angle of $\gtrsim 0.35\pi$, the threshold of the injection effects was $\sim$100 mW, while it was $\sim$20 mW for the detuning angle of 0. In these experiments,

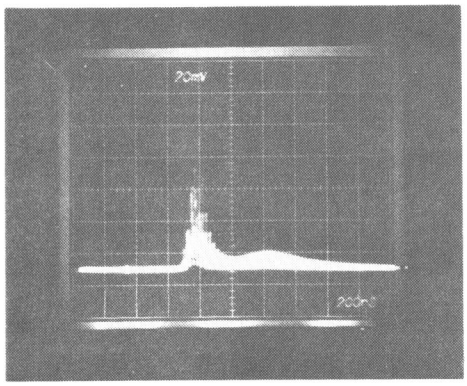

(A)

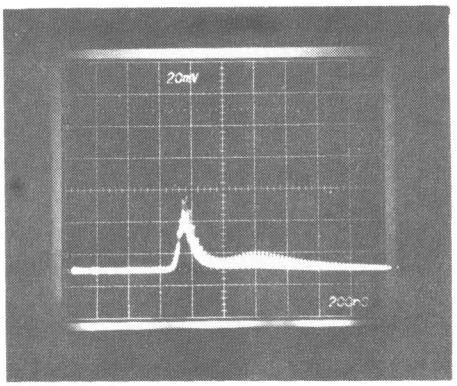

(B)

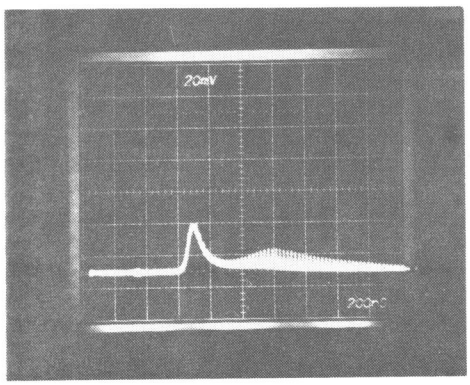

(C)

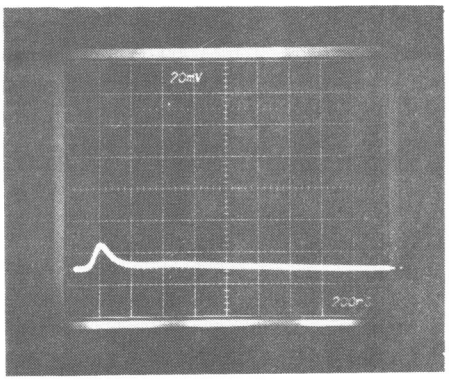

(D)

Fig.3-5. Waveforms of injection line forced oscillation. (A),(B),(C),and (D) correspond to the injection power of 0 mW, $\lesssim$5 mW, $\lesssim$10 mW, and $\sim$ 30 mW respectively. (horizontal scale: 200 ns/div)

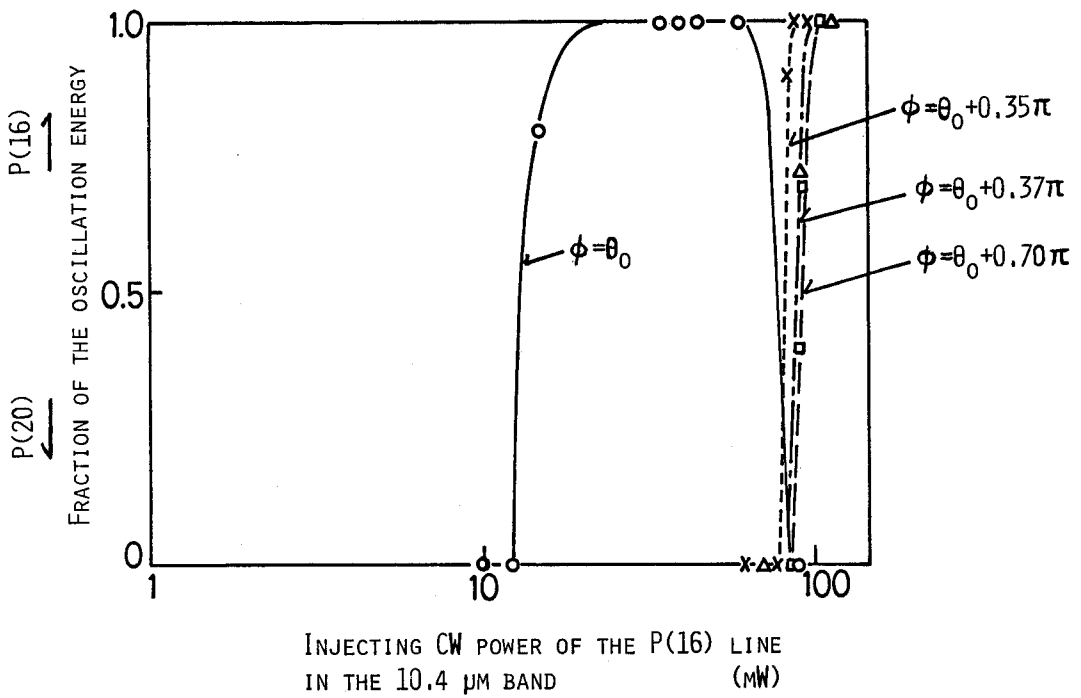

Fig.3-6. Fraction of line forced oscillation energy as a function of the injection cw CO_2 laser power of the P(16) line in the 10.4 μm band.

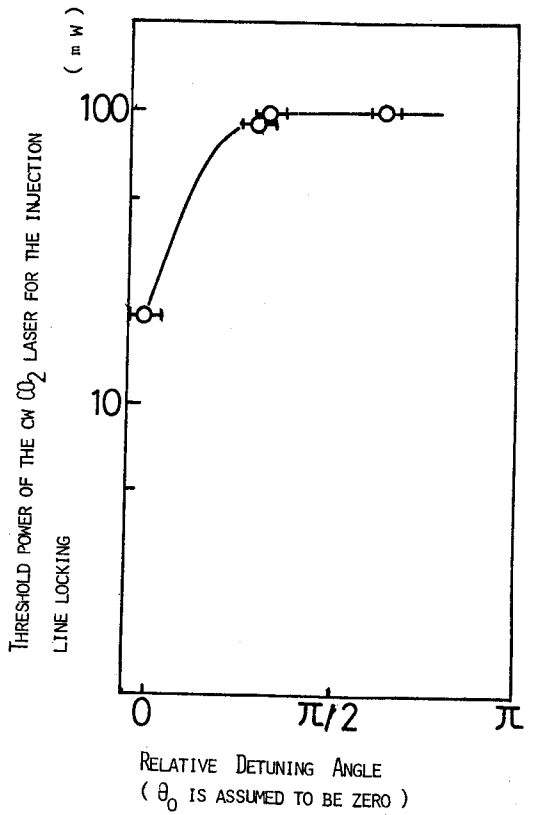

Fig.3-7. Threshold of the injection effect as a function of the relative detuning angle.

the detuning angle at which the injection line forcing effect was quenched, was not found. But the detuning angle at which the injection mode selection could be obtained, was limited within $\sim 0.3\pi$ according to the experimental results obtained by J.L. Lachamber, et al.[5]. Experimental results obtained by the author were not inconsistent with those obtained by J.R. Izatt, et al.[4] and B. Gellert, et al.[5], where no length stabilization or frequency matching between the cw laser and the high power TEA laser was required to obtain reproducible experimental results.

In conclusion, injection line forcing effect had the threshold power of an injecting cw laser, which varied according to the small signal gain of lines and detuning of the longitudinal-mode between the TEA CO_2 laser and the cw CO_2 laser. The thresholds of the injection line forcing effect were measured for the P(16) line of the 10.4 μm band as a function of the detuning angle, and it was confirmed that the angular range where the threshold value decreased was $\lesssim 0.35\pi$. For the angular region of $\gtrsim 0.35\pi$, the thresholds maintained the constant value of 100 mW.

Referances

]). E.J. McLellan and J.F. Figueira, Rev. Sci. Instrum. 50,]213 (1979).

2). C.J. Buczek, R.J. Freiberg, and M.L. Skolnick, Proc. IEEE, 61, 1411 (1973).

3). J.L. Lachamber, P. Lavigne, G. Otiis, and M. Noel, IEEE J. Quantum Electron, QE-12, 756 (1976).

4). J.R. Izatt, C.J. Budhiraja, and P. Mathieu, IEEE J. Quantun Electron, QE-13, 396 (1977).

5). B. Gellert, J. Handke, and B. Kronast, Appl. Phy. 19, 257 (1979).

Chapter 4 Study on short pulse multiline/double-band amplifications

4.1 Introduction

As described in the chapter 1, the (001) upper vibrational level and the (100),(020) lower vibrational levels consist of many rotational sub-levels, and the relaxation time between them is very short. Therefore, energy extraction efficiency from the upper laser level decreases for short pulse saturation-amplifications of the single line amplification, as the duration of energy extraction becomes shorter. To increase the efficiency of the energy extraction for such short pulse saturation amplifications, the multiline amplification is effective. Multiline amplification characteristics in the weakly saturated region have been reported, where the extracted energy density of the multiline amplification did not exceed that of the single line amplification.[1] In this chapter, the saturation characteristics and the improvement in energy extraction in the fully saturating region are described.

Double-band amplifications are also the effective technique to improve the energy extraction efficiency, where the laser transitions occur through both the 9.4 μm band and the 10.4 μm band. If the saturation characteristics for the double-band amplification were compared with those for the single-line/single-band amplification, difference between them contains the effect of double-line amplification. To extract the pure effect of the double-band amplification, the effective saturation energy of the double-band/two-

line amplification was compared with that of the single -band/two-line amplification.

Finally, the amplification characteristics of the modelock pulses having a duration of $\sim$ 1 ns were measured to provide realistic data for a high power short pulse CO_2 laser system.

4.2 Short pulse amplification

A pulse propagation theory for the amplification of single-line nanosecond-duration CO_2 laser pulses has been developed by Schappert.[2] This theory is based on the solutions of a coupled set of rate equations for the photon flux and the rotational level populations. These solutions can be approximated quite well with an effective two-level system with a stored energy density

$$E_{st} = g_o E_s L \qquad 4\text{-}1$$

where g_o and L are the small signal gain coefficient and the active gas length of an amplifier, and E_s is an effective saturation energy density depending on the pulse length and the number of lines or bands in the pulses. The energy extraction in such a model is determined[3] by

$$E_{out} = E_s \ln\{1 + \exp(g_o L)[\exp(E_{in}/E_s) - 1]\} \qquad 4\text{-}2$$

where E_{out} and E_{in} are the output and input energy densities respectively. One can extract the stored energy per unit area for saturating inputs, and it is described by

$$E_{st} = E_{out} - E_{in} = g_o E_s L \quad ; \; E_{in} \gg E_s \qquad 4\text{-}3$$

Thus, to characterize the performance and efficiency of an amplifier, one needs to know only the quantities L, g_o, and the effective saturation energy E_s.

For the laser pulses having a duration of τ_p, the effective saturation energy density E_s can be calculated to be

$$E_s = \frac{h\nu}{2\sigma} g_o L \left(1 - \exp[-\tau_p / \tau_r \, k(J_o)] \right) \qquad 4\text{-}4$$

$h\nu$: photon energy of the CO_2 laser transition of the J_oth upper rotational level.

σ : cross section of stimulated emission for the CO_2 laser transition of the upper rotational level.

g_o : small signal gain coefficient

L : active gas length

τ_p : laser pulse width

$k(J_o)$: reciprocal of the partition fraction of the population for J_oth rotational level calculated by the equation 1-3.

τ_r : rotational relaxation time.

In the fully saturating single band amplifications, only 1/2 of the population inversions between the (001) and the (100) levels or the (001) and the (020) levels can be extracted as the laser emission by pulses sufficiently shorter than the Fermi resonance time, while 2/3 of that can be extracted in case of the fully saturating double-band amplifications by such short pulses. Therefore, the available energy extraction becomes 4/3 times larger by going to double-band energy extraction. Considering that

the ratio R of the $E_s g_o L$ for the double-band (two-line) amplification to that for the single-band (two-line) amplification must be 4/3 and 1 respectively for very short and for very long pulses in comparison with the Fermi resonance time τ_f,[4] R is assumed to be described by

$$R = \frac{1}{1-\frac{1}{4}\exp(-\tau_p/\tau_f)} \qquad 4\text{-}5$$

for the laser pulse having a duration of τ_p.

4.3 Multiline amplification of 3 ns pulses

The experimental apparatus is illustrated in Fig.4-1. The output pulse of the gain-Q-switching multiline oscillator described in the chapter 2 was pulse-shaped by a double Pockels cell to obtain three nanosecond pulses with a signal-to-noise ratio greater than 10^4. In order to increase the input energy density and observe the saturation characteristics clearly, a three-path amplification optical system was constructed using a 1 atm electron-beam-controlled amplifire. The active gas length was 800 mm per path. The mixing ratio was CO_2:N_2:He = 1:1:3. Apertures were placed on each power monitor to cut off the unsaturated region of the laser beam and to determine the energy density of the laser beam accurately. The spectra of the amplified laser beam were recorded on heat sensitive films using a grating and focussing optics. They were the P(20), P(18), P(14), R(14), R(16), R(18), and R(20) lines in the 10.4 μm band and the P(18) and P(20) lines in the 9.4 μm band.

The experimental results are shown in Fig.4-2. The

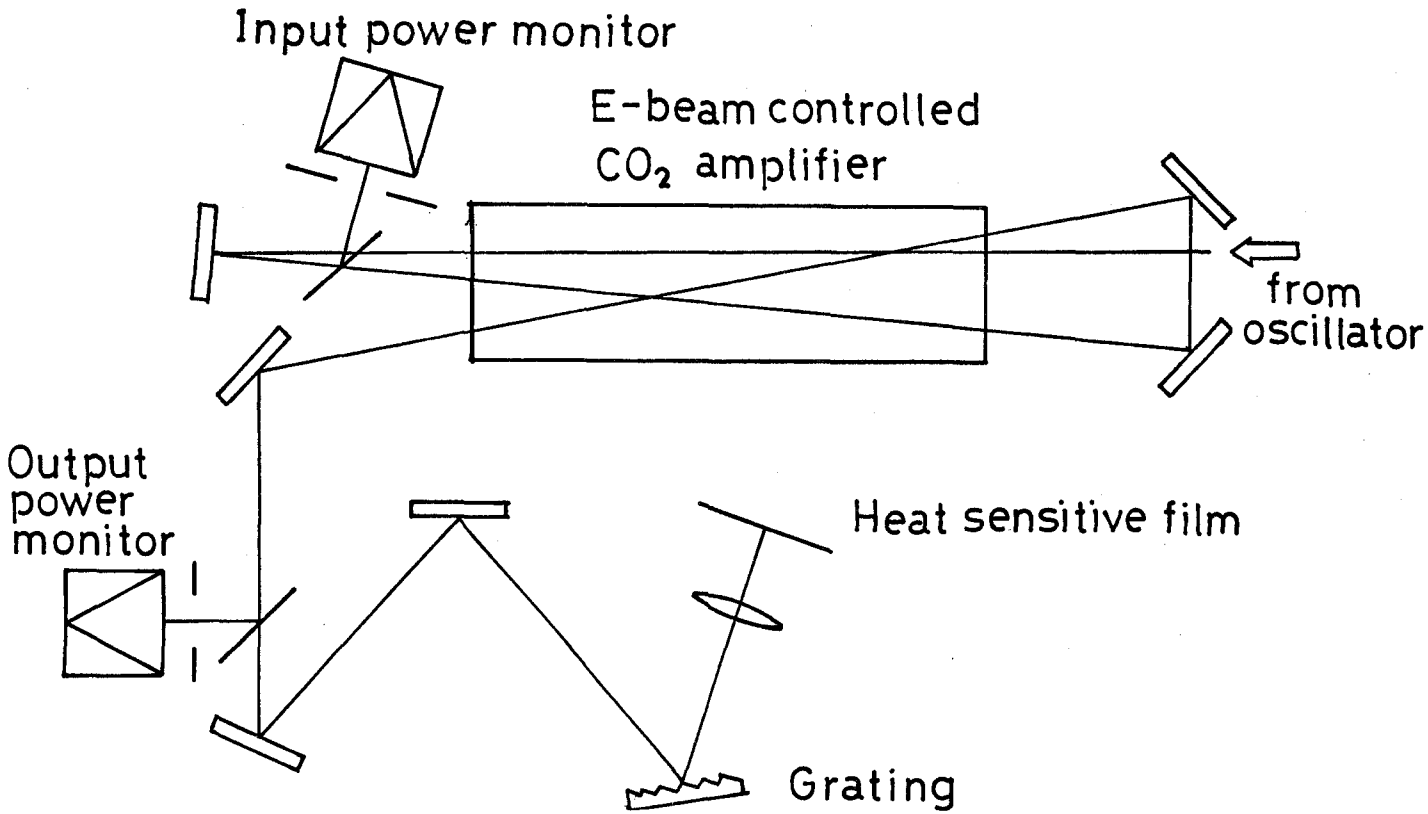

Fig.4-1. Experimental apparatus for short pulse multiline amplification.

single-line pulse saturates at lower input energy density than the multiline pulse. It is observed that the multiline extracted energy clearly exceeds that of the single-line pulse at the P(20) line in the high input energy density region.

Substituting various pairs of E_s and g_o into the equation 4-2, the best fit curves to the experimental data were found. These are the solid curves shown in Fig. 4-2. For multiline amplifications, E_s = 120 mJ cm^{-2} and g_o = 2.4 % cm^{-1}, while E_s = 43 mJ cm^{-2} and g_o = 3.0 % cm^{-1} for single-line amplifications. $E_s g_o$ increased by a factor of 2.2 for nine-line amplifications.

4.4 Double band amplification of 3 ns pulses

The experimental apparatus is shown in Fig.4-3. A gaseous absorber method was used to obtain double band oscillations. A mixture of SF_6, C_2F_5Cl, and C_2H_5OH was used as the absorber gas. These gases absorbed the P branch in the 10.4 μm band, the R branch in the 10.4 μm band, and the P and R branches in the 9.4 μm band respectively. An etalon plate was used to select the oscillation lines as described in the chapter 2. The output pulse of the gain-Q-switching oscillator was pulse shaped by a double Pockels cell to obtain 3 ns pulses in the FWHM with a signal to noise ratio better than 10^4. These pulses are amplified by pre-amplifiers to be $\sim$ 100 mJ. To increase the energy density, a confocal mirror pair was used and the beam diameter was decreased. The amplifier used for the measurement of the saturation characteristics was a TEA CO_2 laser. The

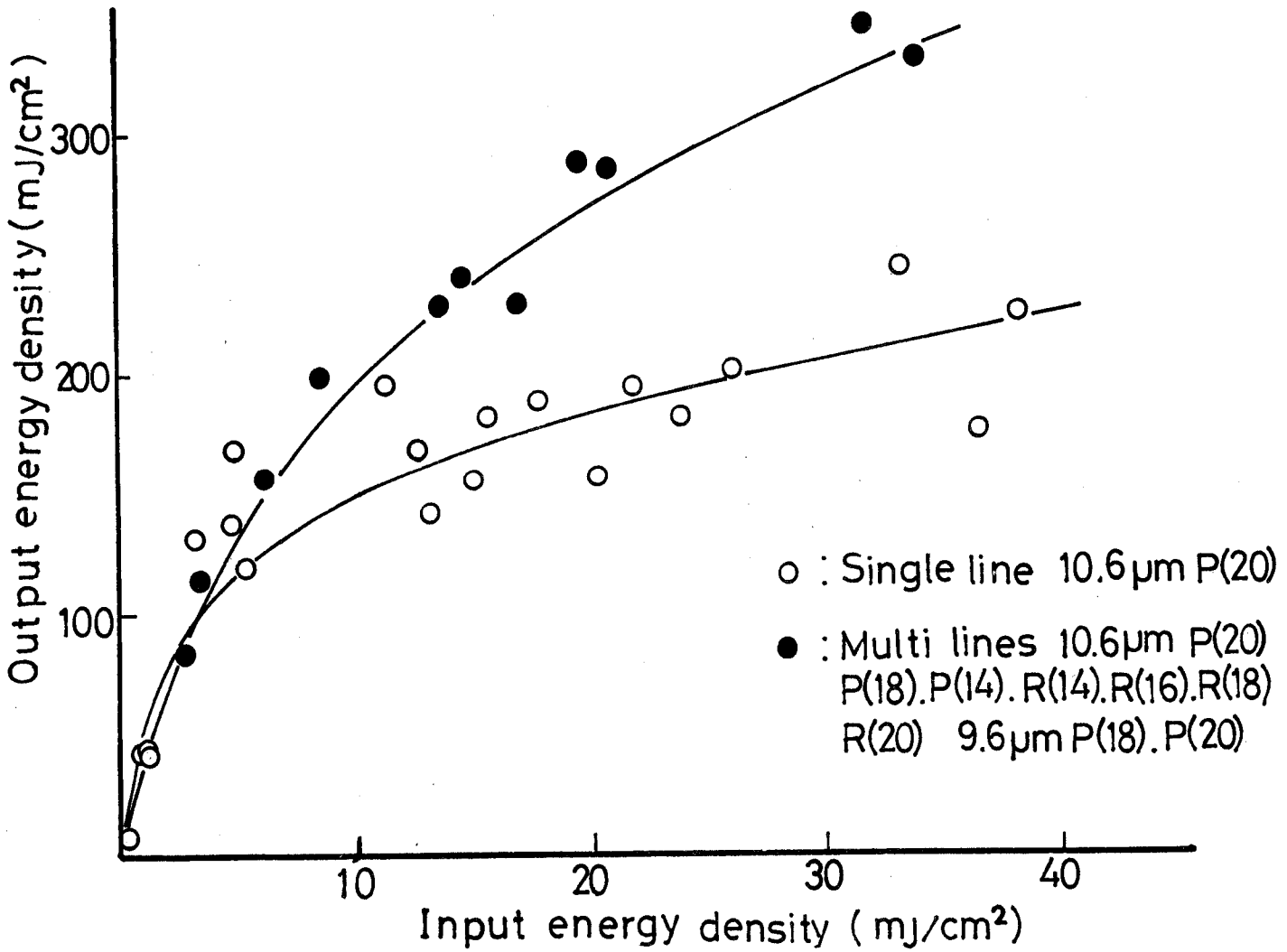

Fig.4-2. Saturation characteristics of multiline amplifications for 3-ns pulse.

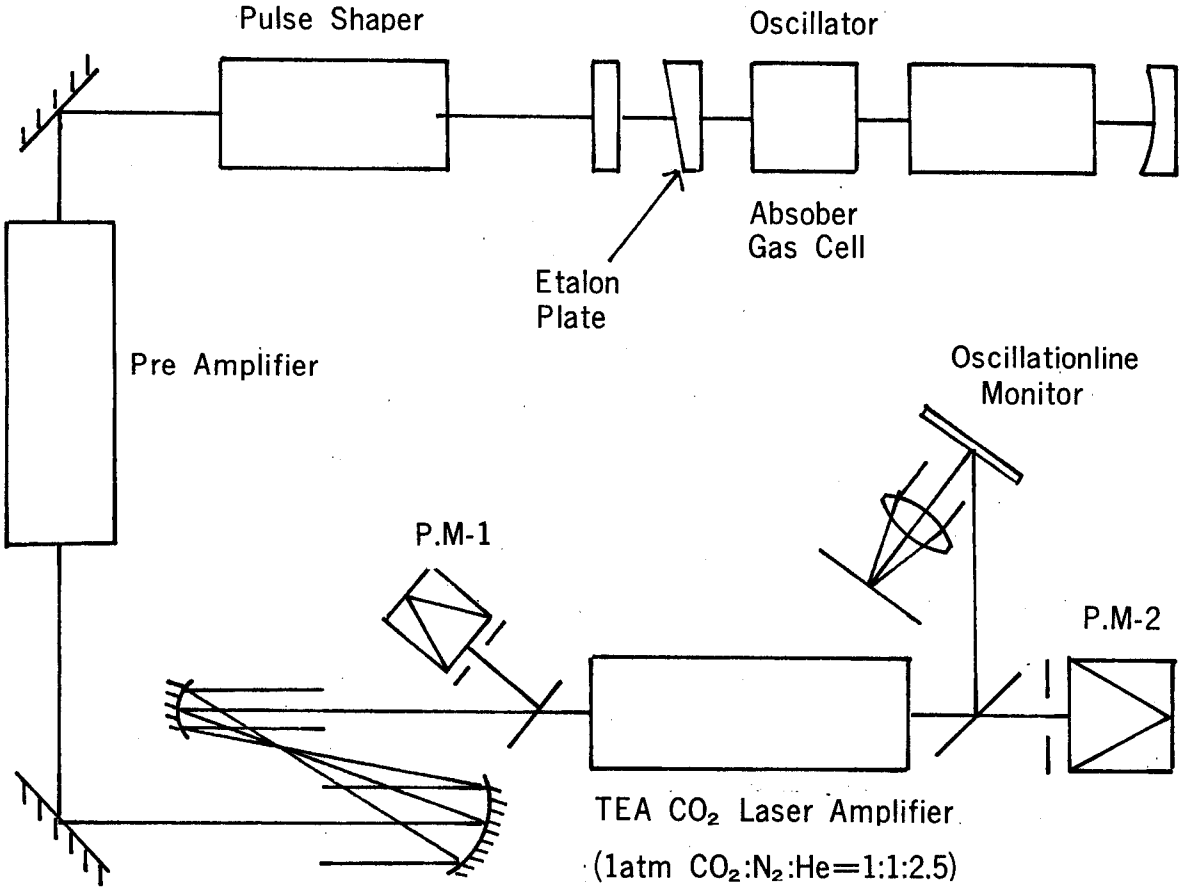

Fig.4-3. Experimental apparatus for short pulse double band amplifications.

mixing ratio of the laser gas was CO_2 : N_2 : He = 1 : 1 : 2.5. Input energy density and output energy density were measured by PM-1 and PM-2 respectively. Apertures were placed in front of these calorimeters to select uniform energy density regions of the laser beams. The output laser beam was splitted out and its spectra were recorded on the heat sensitive films by a focussing optics and a grating.

Before measuring the double-band amplification characteristic single band amplification characteristics were measured for the 10.4 μm band and the 9.4 μm band respectively. These are shown in the Fig.4-4. Black circles and open circles denote the 10.4 μm band and the 9.4 μm band respectively. By using the equation 4-2, the effective saturation energies (E_s) and the small signal gains (g_o) were determined. For the 10.4 μm band amplification, E_s and g_o were 90 $mJcm^{-2}$ and 0.039 cm^{-1} respectively, and for the 9.4 μm band amplification, E_s and g_o were 104 $mJcm^{-2}$ and 0.03 cm^{-1} respectively. The small signal gain coefficient g_o for the 9.4 μm band was about 20 % smaller than that for the 10.4 μm band, which coincides with the measurement by S. Singer.[5]

Saturation characteristics for the double-band two line amplification and the single-band two-line amplification are shown in Fig.4-5. The former and the latter are denoted by black circles and open circles respectively. The best fit curves to the experimental data were obtained by changing E_s and g_o of the equation 4-2. For the double-band two-line amplifications, E_s and g_o were 121 mJ cm^{-2} and 0.035 cm^{-1} respectively, while E_s and g_o were 92 $mJcm^{-2}$ and 0.037 cm^{-1} respectively for the single-band two-line amplification.

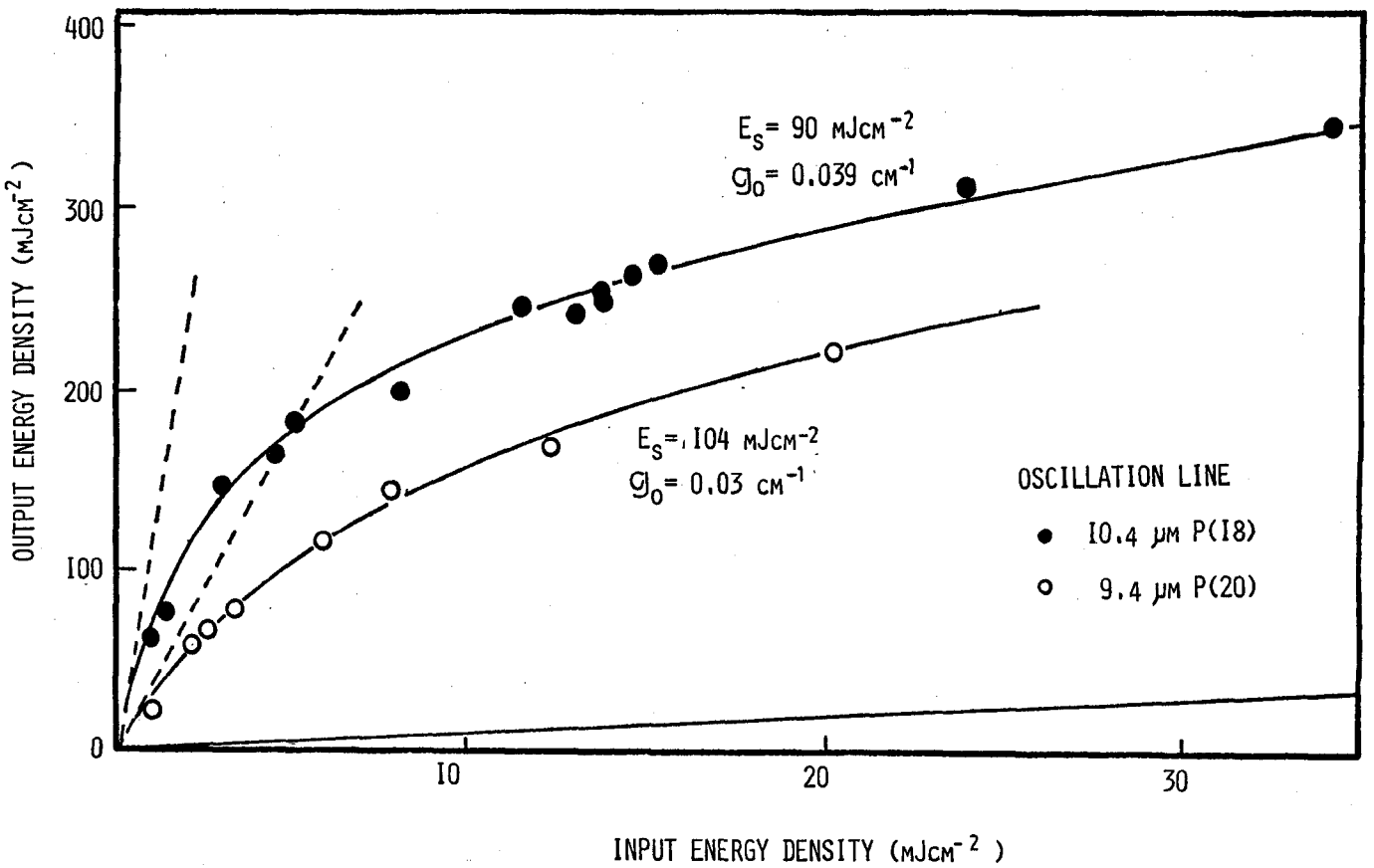

Fig.4-4. Saturation characteristics of single band amplifications.

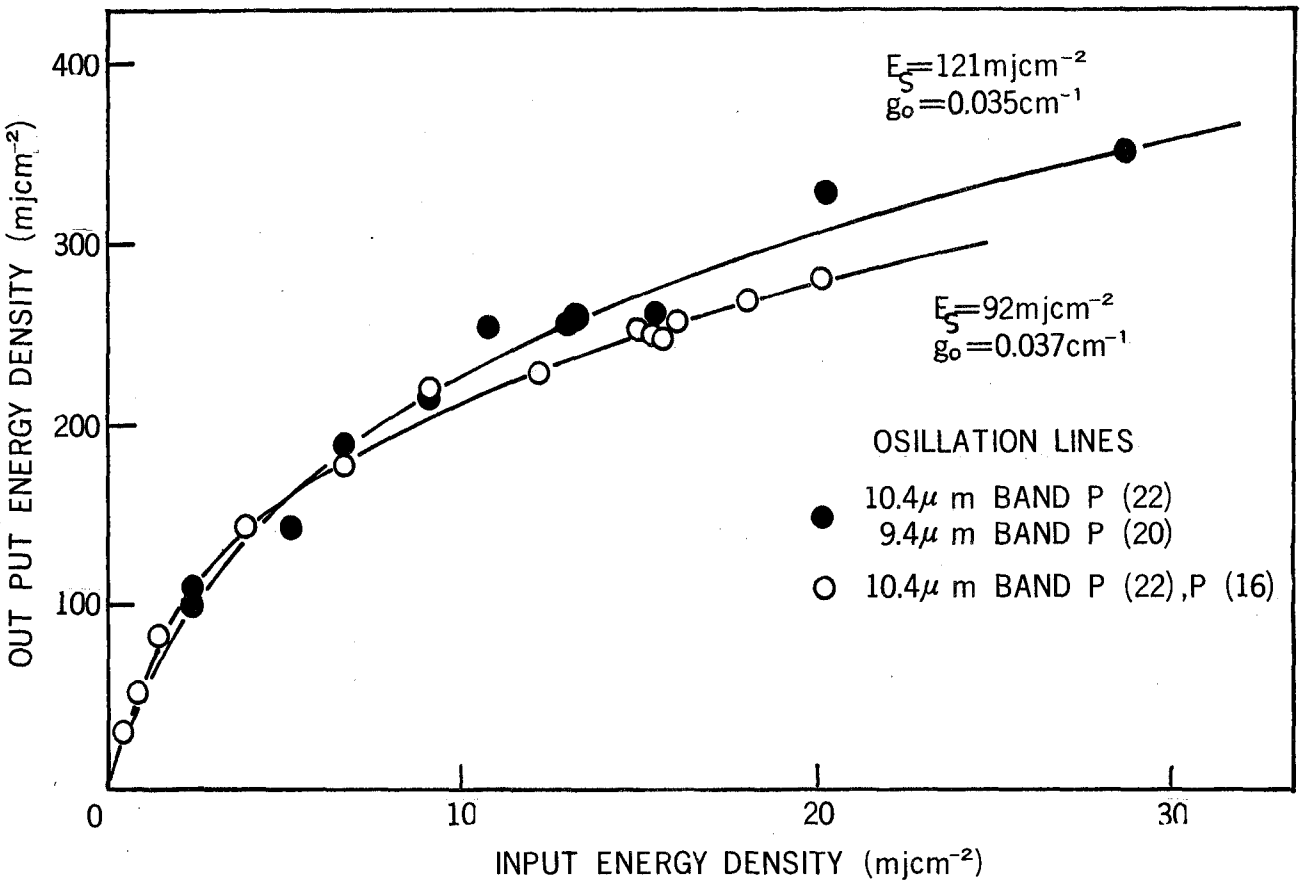

Fig.4-5. Saturation characteristics of double band two line amplifications and single band two line amplifications.

$E_s g_o L$ increased 24.5 % by going effectively to the double-band amplification from the single-band amplification.

In this measurement, the increase in $E_s g_o L$ did not reach to 33 % as expected in the introduction of this chapter. This can be explained by the innegligible duration of energy extraction in comparison with the Fermi resonance time τ_f. By using Jacobs's experimental result,[4] the resonace relaxation time between the (100) and the (020) levels (τ_f) can be calculated to be 7.4 ns for the gas mixture of CO_2 : N_2 : He = 1 : 1 : 2.5. By substituting τ_p = 3 ns, τ_f = 7.4 ns into the equation 4-5, r = 1.20 can be obtained which corresponds to the increase of 20 % and roughly agrees with the experimental results.

4.5 Multiline amplification of ~ 1 ns pulses

In this section, the amplification characteristics of modelock pulses having a duration of 1.2~ 1.5 ns by a He-free [6] electron-beam controlled amplifier were presented in the fully saturating output energy region, which will provide realistic data for a short pulse high power laser system.

The experimental apparatus is shown in Fig.4-6. Short pulses having a duration of 1.2~1.5 ns were produced by the modelock TEA CO_2 laser oscillator described in the chapter 2. These were amplified upto 100mJcm^{-1} by pre-amplifiers and by the first path of an electron-beam controlled CO_2 laser amplifier with the active gas length of 1 m. The total pressure of the laser gas was 1.2 atm and the mixing ratio of CO_2 : N_2 : H_e was set at 1 : 1/4 : 0. Input and output energies were monitored by two calorimeters (CM). In the two

line amplification experiment using the P(20) line and the P(14) line in the 10.4 μm band, power spectrum analyzers (SA) described in the chapter 2 were used to measure the energy distribution of the P(20) and P(14) lines. Apertures were placed in front of each energy monitor to pull out the central portion of the beam where the energy density was uniform. Wave forms of the laser beams were monitored by a photon drag detector (PD) placed at the exit of the amplifier. The electrical input energy into the amplifier was 340 mJ cm^{-3}, and the small signal gain coefficient g_o was 5.5 $\%cm^{-1}$ which was measured in an another experiment. Fig.4-7 shows the change in the energy density fraction of the P(20) line in the input and output energy densities. It can be seen that the energy density fractions of the P(20) and the P(14) lines have the tendency to approach the same value of $\sim$ 0.5 by saturation amplification.

The experimental results of the fully saturating amplifications are shown in Fig.4-8. Black circles denote the two-line amplification of the P(20) and P(14) lines in the 10.4 μm band. In these data points, the amplification where the output energy density fraction of the P(20) line was larger than 70 % or smaller than 30 %, was not included. Open circles represent the single-line amplification of the P(20) line in the 10.4 μm band. There were not significant differences between the saturation characteristics of the single-line amplifications and those of the multiline amplifications, even in the high input energy density region. Using the equation 4-2 and g_o= 5.5 % cm^{-1}, E_s could be determined to be 175 $mJcm^{-2}$ for the amplification of the

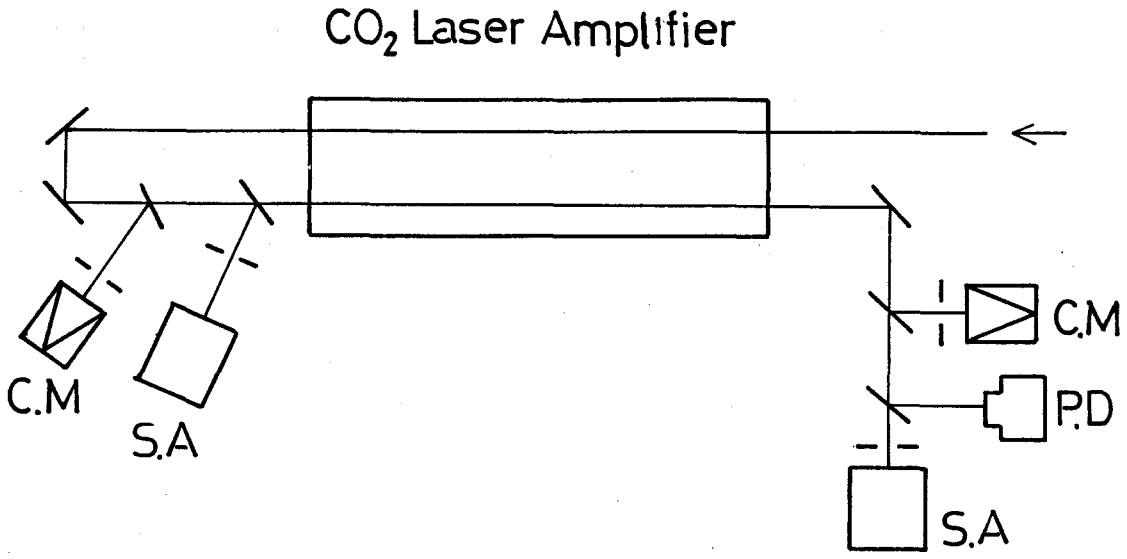

Fig.4-6. Experimental apparatus for the multiline amplifications of 1 ns pulses in the fully saturation output energy density region.

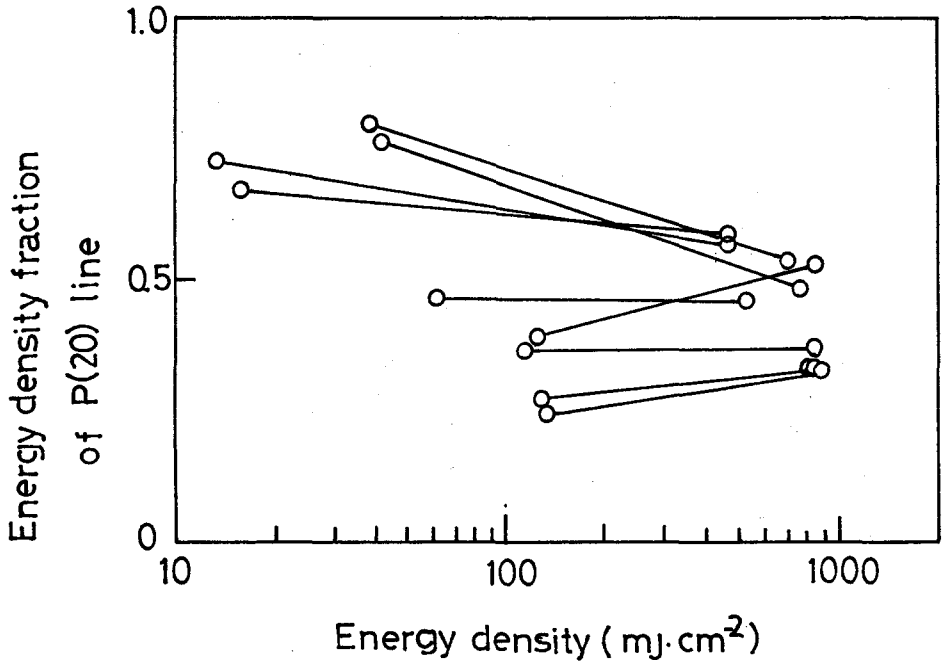

Fig.4-7. Energy density distribution of the P(20) and P(14) lines for the input and output laser pulses.

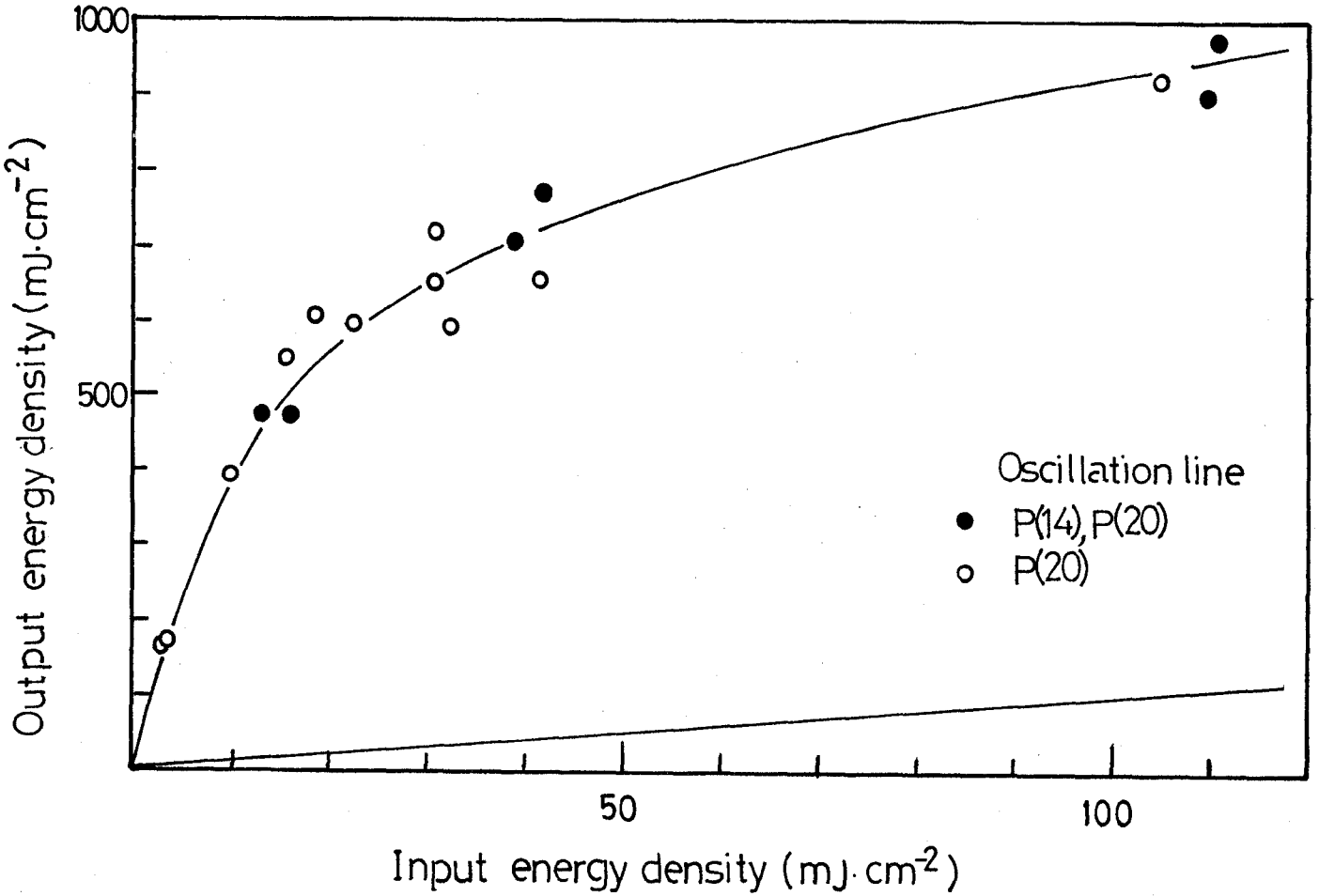

Fig.4-8. Saturation characteristics of 1 ns pulse amplifications in the fully saturating output energy density region.

P(20) line. Assuming the gas temperature of 400 K, the effective small signal gain coefficient for the two-line amplification, which can be obtained by averaging those for the P(20) and P(14) lines, can be calculated to be 5.2 %. Using this value, E_s could be determined to be 188 $mJcm^{-2}$ for the two-line amplification of the P(20) and P(14) lines. From the absorption data, the cross section for stimulated emission in pure CO_2 at 1 atm can be calculated to be $\sigma_o = 1.05 \times 10^{-18}$ cm^2 for the P(20) line in the 10.4 μm band.[7] This must be corrected [7,8] for foreign gas broadening by

$$\sigma = \sigma_o / P[1 \times F(CO_2) + 0.73 \times F(N_2) + 0.6 \times F(He)] \qquad 4\text{-}6$$

where $F(CO_2)$, $F(N_2)$, and $F(He)$, are the mole fractions of CO_2, N_2 and He respectively, and P is the total pressure. For the gas mixture used in this experiment, σ can be calculated to be $9.25 \times 10^{-19} cm^2$. τ_r in pure CO_2 at 1 atm (τ_{ro}) can be calculated to be 0.12 ns from the measurement at a few torrs.[9] τ_r at P atm can be corrected[10] by

$$\tau_r = \tau_{ro} / P\{1 \times F(CO_2) + 0.9 \times F(N_2) + 0.63 \times F(He)\} \qquad 4\text{-}7$$

and calculated to be 0.098 ns for the gas mixture used in this experiment. Assuming the gas temperature of 400 K, $k(J_o)$ is 14.7 and 13.1 for the P(20) line and the P(14) line respectively. Substituting these values into the equation 4-4, E_s can be calculated to be 96.4 $mJcm^{-2}$ and 128 $mJcm^{-2}$ for the single line amplification of the P(20) line and the

two-line amplification of the P(20) and P(14) lines respectively. $k(J_o)$ was corrected by $k(J_o)=1/14.7 + 1/13.1$ for the two-line amplification. Not only the absolute values but also the difference between these two E_s did not coincide with the experimental results. If 2.5 τ_r is used in place of τ_r in the equation 4-4, E_s can be calculated to be 138 mJ/cm^2 and 148 mJ/cm^2 for the single-line and two-line amplifications. In this case, the increase ratio of E_s coincides with that of experimental results, but the absolute values of E_s are still smaller than E_s obtained in the experiment. The reason why such large E_s could be obtained is being investigated.

4.6 Summary

Increase in the energy extraction was demonstrated by using nine-line amplification of 3 ns pulses. Increase in the effective saturation energy by going to double-band amplification was shown comparing double-band two-line amplification with single-band two-line amplification. This increase was suppressed by the Fermi resonance between the lower (100) and (020) levels, and the amount of suppression was explained quantitatively. Saturation characteristics of 1 ns multiline pulses through a He-free electron beam controlled CO_2 laser amplifier were measured to obtain realistic data for constructing a high power CO_2 laser system. Large effective saturation energy was obtained even for single-line amplification of the P(20) line. This exceeded the theoretical value calculated by using the cross section of stimulated emission.

Referances

1). J.F. Figueira, J.S. Ladish, G.T. Schappert, and S.J. Thomas, Appl.Phys. Lett. 27, 591 (1975).

2). G.T. Schappert, Appl. Phys. Lett. 23, 319 (1973).

3). L.M. Frantz and J.S. Nodvik J. Appl. Phys. 34, 2346 (1963).

4). R.R. Jacobs, K.J. Pettipiece, and S.J. Thomas, Phys. Rev. A 11, 54 (1975).

5). S. Singer, IEEE J. Quantum Electron QE-10 829 (1974).

6). K. Okamura, H. Fujita, M. Matoba, S. Nakai and C. Yamanaka, Technology Reports of the Osaka University, 29, 449 (1979).

7). T.K. McCubbin, Jr. and T.R. Mooney, J.Quant.Spectrosc. Radiat. Transfer, 8, 1255 (1968).

8). R.R. Patty, E.R. Manring, and J.A. Gardner, Appl. Opt. 7, 2241 (1968)

9). P.K. Cheo and R.L. Abrams, Appl. Phys. Lett. 14, 47 (1969).

10). R.L. Abrams and P.K. Cheo, Appl. Phys. Lett. 15, 177 (1969).

Chapter 5. Study on plasma shutters.

5.1 Introduction.

In target irradiation experiment using extremely high power short pulse lasers, a part of the laser beam incident on a target is reflected by the plasma on the target surface. This retropulse is amplified passing through the amplifier chain back, and the energy becomes large enough to cause optical damages on the optical components. To prevent these optical damages, a uni-directional coupler such as a Faraday rotator [1] may be introduced into the amplifier chain. For CO_2 lasers, whose wavelength is 10.6 μm, there is no suitable Faraday element having a Verdet constant sufficiently high to construct a large aperture optical shutter. The construction of the plasma shutter, which can take place of the Faraday rotator, is very important not only for the target irradiation experiments but also for the construction of the inertial confinement fusion reactor system where the CO_2 laser may be used as a driver. From these points of view, three types of plasma shutters, such as a plastic thin film plasma shutter, an air discharge plasma shutter, and a laser-induced plasma shutter were developed and their characteristics were studied.

5.2 Plastic thin film plasma shutter

The simplest method to prevent a retropulse is a plastic $[(C_{10}H_8O_4)_n]$ thin film plasma shutter.[2] The outgoing laser pulse produces plasma on the plastic thin film placed on the beam waist of the laser beam. Fig.5-1 shows the transmission

of the plastic thin film plasma shutter as a function of the energy density on the thin plastic film (3 μm). Pulse duration was 3 ns. Germanium lens with the focal length of 140 mm was used to focus the laser beam on the film. Focussing diameter was $\sim$ 0.6 mm. For high input energy density of $\gtrsim 10^5$ mJ/cm^2, small transmission less than 10 % was obtained. For low input energy density of $\sim 10^3$ mJ/cm^2, transmission larger than 90 % was measured. Fig.5-2 (a),(b) show the waveforms of a 3 ns (FWHM) input laser pulse and the transmitted laser pulse respectively, when the input power density on the plastic thin film was $\sim 3 \times 10^{10}$ w/cm^2. Fig.5-3 (a),(b) show the waveforms of a 70 ns (FWHM) input laser pulse and the transmitted laser pulse respectively, when the input power density was $\sim 1.5 \times 10^8$ w/cm^2. The laser pulse was cut off at the tail after the peak of the input laser beam. These experimental results show that the attenuation of the laser beam through the thin film shutter is a function of the incident power and its waveform. Laser beams of short pulse width can pass through it without pulse deformation when the power level is below threshold value. High power laser beam such as amplified retro-pulse can be cut off to very low level of transmission.

5.3 Air discharge plasma shutter

As shown in the previous section, the plastic thin film plasma shutter does not have high attenuation ratio for a weak laser pulse. An active plasma shutter which is making use of air discharge plasma, was developed and its characteristics were studied. N.H. Burnett, et al [3] suggested that an

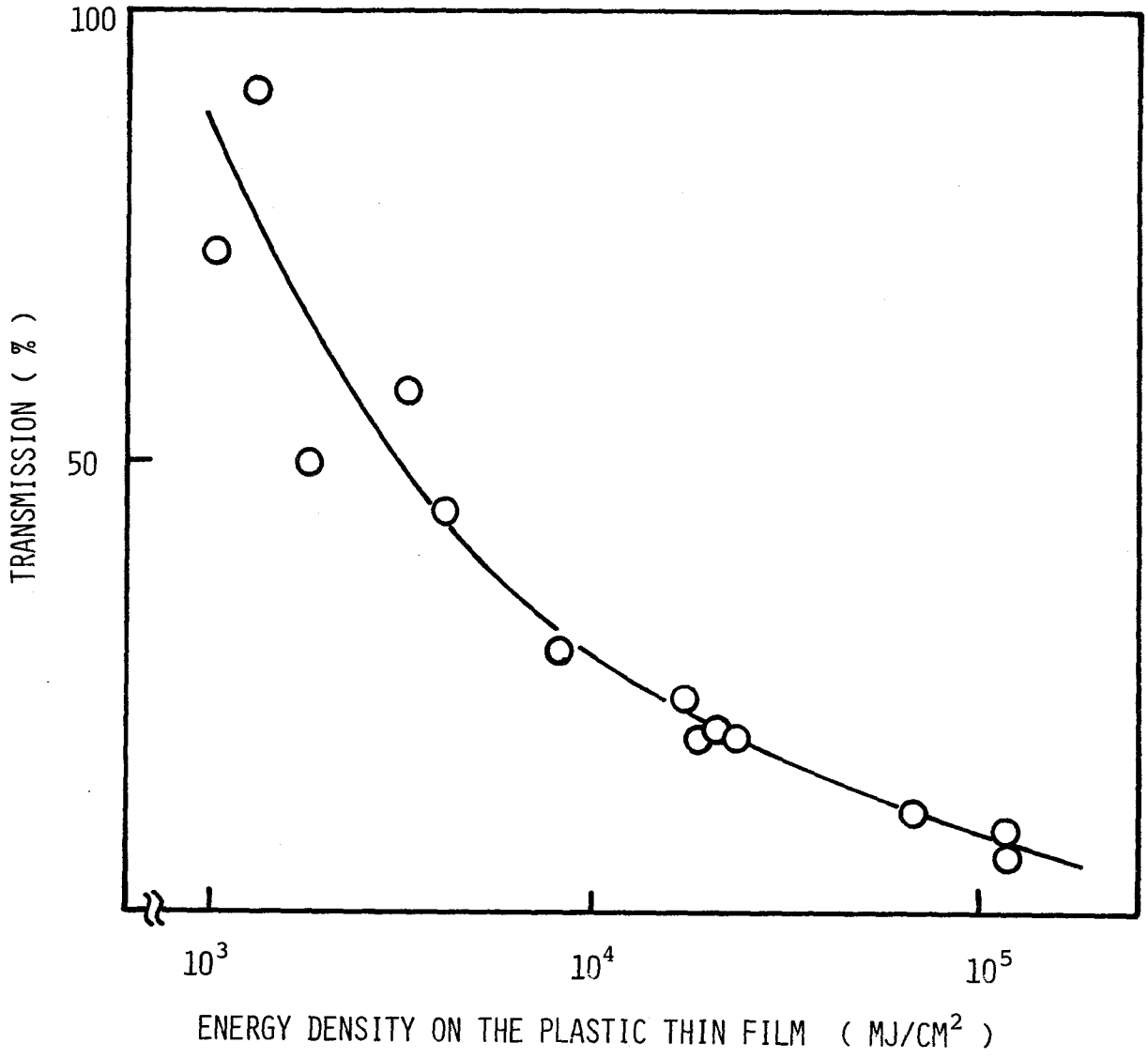

Fig.5-1. Transmission of the plastic thin film plasma shutter as a function of the laser energy

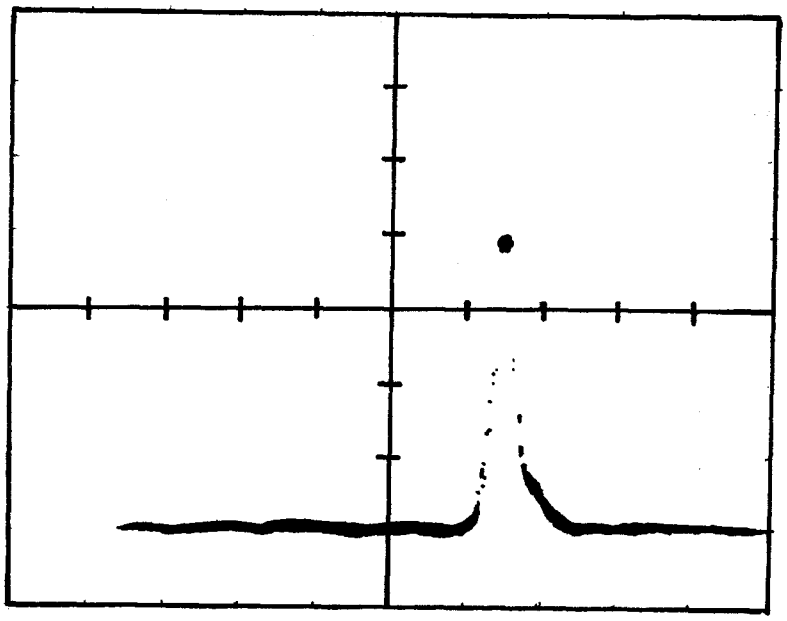

Fig.5-2 (a). Waveform of the input laser pulse having a duration of 3 ns in the FWHM. (horizontal scale: 5 ns/div, vertical scale: 20 mV/div)

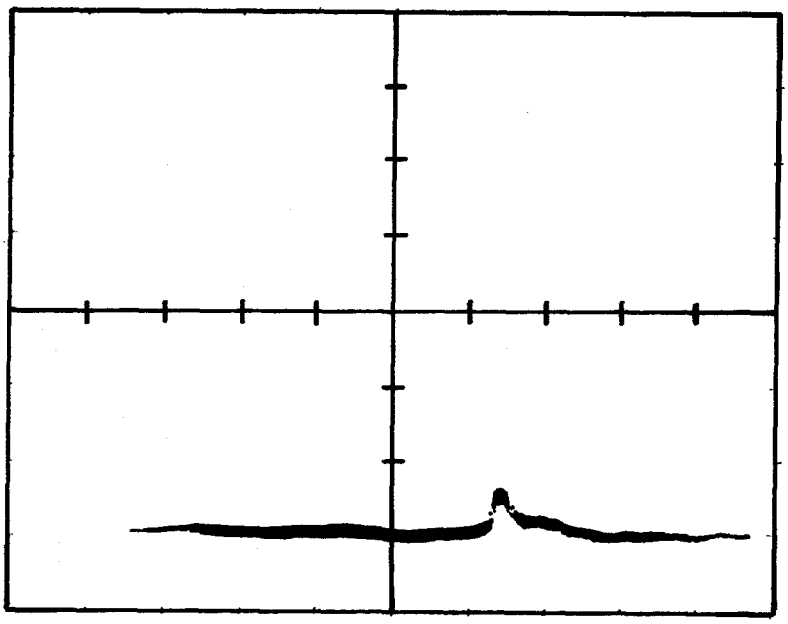

Fig.5-2 (b). Waveform of the output laser pulse. (horizontal scale: 5 ns/div, vertical scale: 5 mV/div)

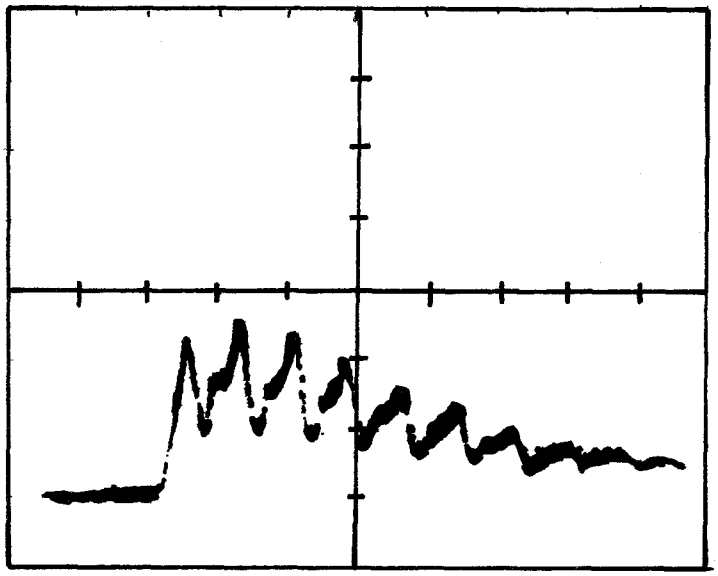

Fig.5-3 (a). Waveform of the input laser pulse. (horizontal scale: 20 ns/div)

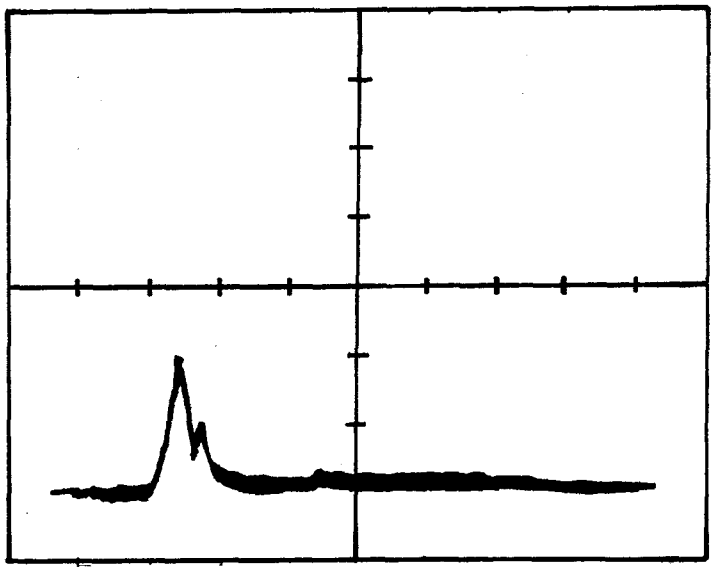

Fig.5-3 (b). Waveform of the transmitted laser pulse through the plastic thin film plasma shutter. (horizontal scale: 20 ns/div)

electrically induced plasma column in air could provide significant attenuation for a CO_2 laser beam. In their experiments, high attenuation was obtained when a high power CO_2 laser was focussed onto the plasma column by a cylindrical mirror. P. Weiss[4] demonstrated that the spark initiated plasma acted as a seed plasma for a gas break down by the laser beam, and there was a trend of increasing attenuation with increasing incident laser power. Beside these applications of the air discharge plasma column, S. Ishii and B. Ahlborn[5] showed that it could be used as an optically active element for a Q-switching.

The experimental setup is shown in Fig.5-4. A laser beam of 3 ns (FWHM) in duration and 20 mJ in energy was focused onto the plasma column between the electrodes of the air discharge plasma shutter. The beam diameter was 20 mm. The focal spot size was estimated to be $\sim$0.6 mm in diameter by a heat sensitive film placed at a focal point. The electrodes of the air discharge plasma shutter had conical shapes and the distance between them was 2 mm. To maintain a constant current discharge with fast rise, coaxial cables were used as a transmission line type capacitor and charged to 12 kV. A thyratron was used to short one end of the cable. Total length of the cable was 200 m. The discharge current and the duration were 240 A and 2 μs respectively as shown in Fig.5-5. The relative timing between the start of the discharge and the arrival of the laser beam at the plasma column was changed arbitrarily by an electronic delay circuit with an accuracy of 50 ns. The incident energy, the transmitted energy, and the reflected energy by the

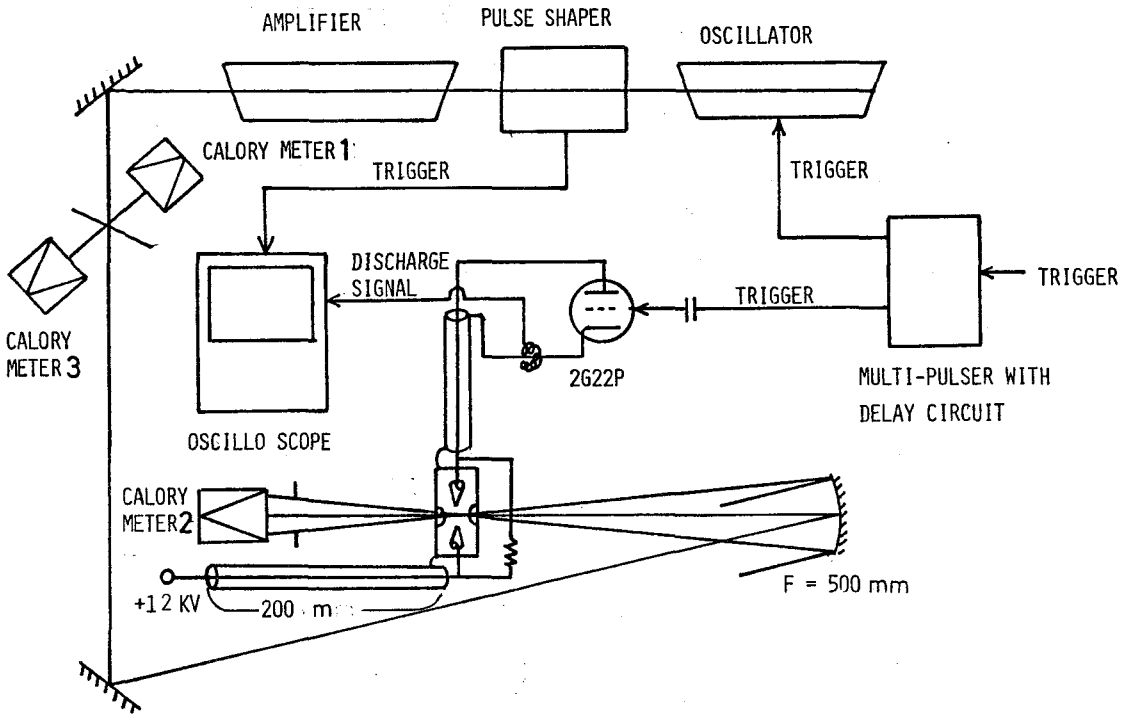

Fig.5-4. Experimental apparatus of the air discharge plasma shutter.

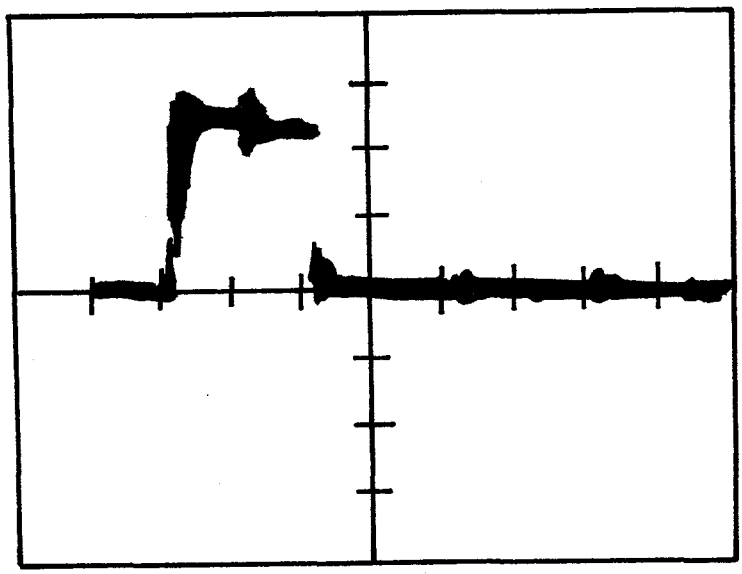

Fig.5-5. Waveform of the discharge current (horizontal scale: 1 μs/div, vertical scale: 0.5 V/div, 1 V corresponds to 200 A)

plasma column were monitored by calory meters 1,2, and 3 in Fig.5-4 respectively.

The transmission characteristics of the probe laser beam through the plasma column is shown in Fig.5-6 as a function of the interval between the start of the discharge and the arrival of the laser beam at the plasma column. The distance between the axis of the plasma column and that of the probe laser beam (D) was changed to see the effective region for attenuation. For D = 0 mm, the transmission decreased sharply just after the start of the discharge and became its minimum value of 2 % at 0.15 μs. Then the transmission increased gradually, though the constant current discharge was maintained for 2 μs. For D = 0.6 mm, the transmission started to decrease just after the start of the discharge and reached gradually its minimum value of 3 %. Assuming that the decrease of transmission is due to the arrival of the front of the plasma column traversing through the focal spot size of 0.6 mm, the expansion velocity is calculated to be 8.6×10^2m/s from the slope of the curve. For D = 0.9 mm, an increase of 0.3 mm in D introduces an initial transparent period of 0.35 μs as shown in Fig.5-6. From this period, the expansion velocity of the plasma column is also estimated to be 8.6×10^2m/s, which agrees with the value obtained from the slope of the transmission decrease. Attenuation characteristics of the air discharge plasma shutter is shown in Fig.5-7 as a function of the input laser energy. For small input laser energy ($\lesssim$1 mJ) the transmission was approximately more than 5 times larger than that for higher input laser energy ($\gtrsim$15 mJ). This

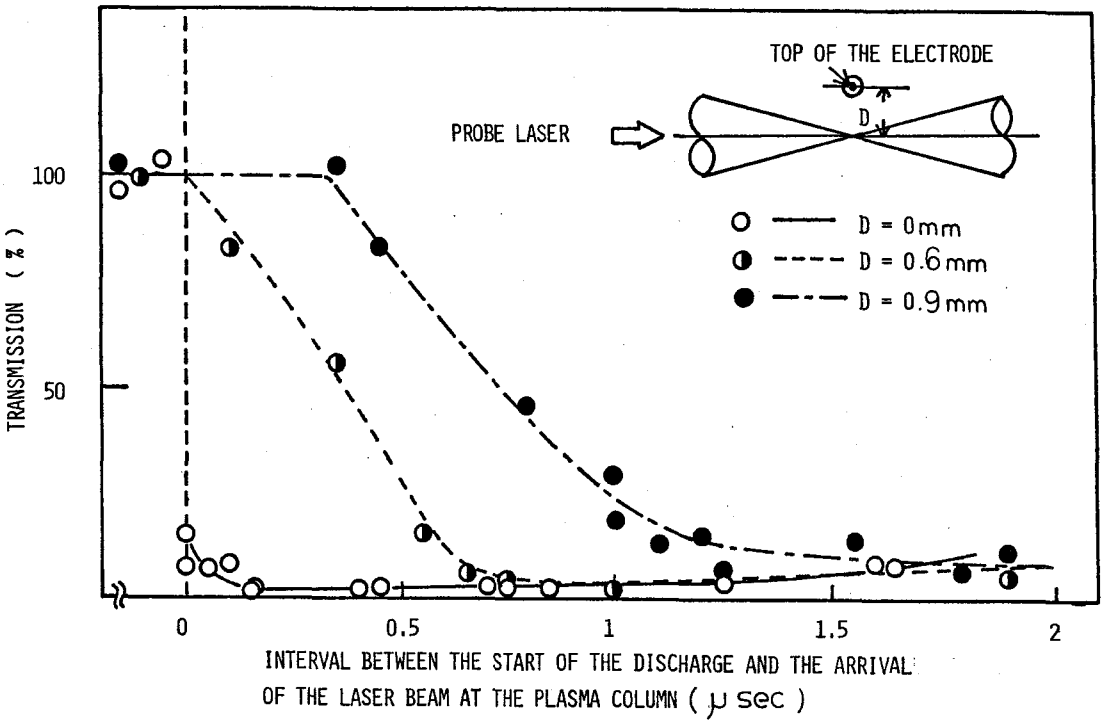

Fig.5-6. Transmission of the air discharge plasma column as a function of the delay time (interval between the start of the discharge and the arrival of the laser beam at the discharge plasma column)

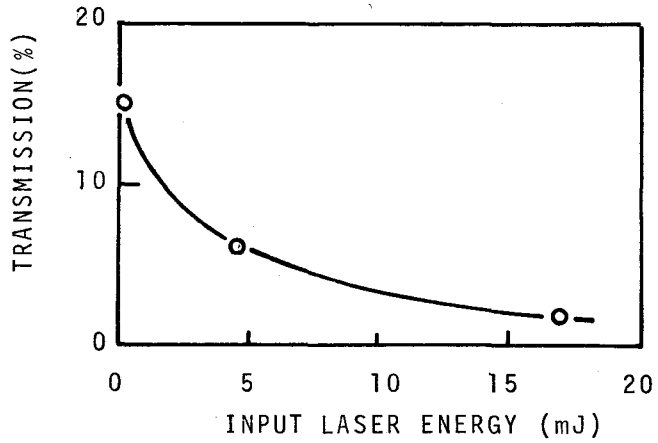

Fig.5-7. Attenuation characteristics of the air discharge plasma column as a function of the input laser energy.

means that the attenuation of the air discharge plasma shutter is caused not only by the air discharge plasma column, but also by the laser induced plasma seeded by electrical discharge.

To see the influence of the ambient disturbance, such as shock waves which might precede the expansion of the plasma column, a similar experiment was done using a cw He-Ne laser as a probe laser light instead of a CO_2 laser. In this experiment, any attenuation of transmission was not observed. Considering that the refractive index of neutral gas is larger for the shorter wave length light, the observed effect on CO_2 laser beam is not caused by the refraction of the ambient air.

Radiation from the plasma column was measured by a photo-multiplier and a Tektronix 7904 oscilloscope. The radiation from the center of the plasma column is shown in Fig.5-8(a),(b). Very fast rise of less than 20 ns was observed.

To see the profile and the dynamic behavior of the plasma column, calory meter 2 in Fig.5-4 was replaced by a pyro-vidicon camera, and shadow-grams were taken by using the 3 ns CO_2 laser pulse as an illuminating light as shown in Fig.5-9(H). In this case, the plasma column was produced 30 mm away from the focal point (The beam diameter was 6mm on the surface of the pyro-vidicon camera.). So the magnification ratio was 6. For this measurement, the amplifier was not used, therefore the laser beam energy was less than 0.1 mJ. The experimental results are shown in Fig.5-9. Fig.5-9 (A) shows the beam profile of the CO_2 probe laser. Fig.5-9(B)

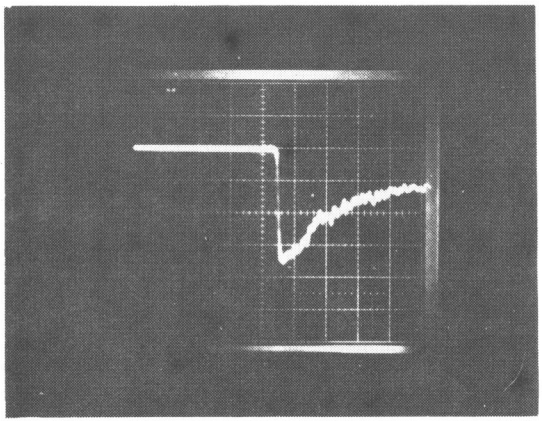

(a)

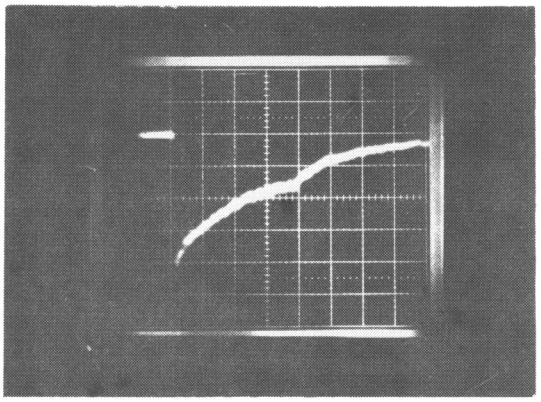

(b)

Fig.5-8. Radiation from the center of the plasma column. (a); Horizontal scale is 100 ns/div. (b); Horizontal scale is 500 ns/div.

shows a shadow of the plasma column at 0.05 μs after the start of the discharge. The diameter of the plasma column was 0.4 mm. Fig.5-9(C) shows a shadow at 0.25 μs. The transmitted region appeared around the central part of the beam which was due to the reduction of the plasma density. Fig.5-9(D),(E),(F), and (G) show shadows at 0.35 μs 0.45 μs, 0.75 μs and 1.2 μs respectively. The transmitted probe laser beams were spread horizontally. The transmitted beam profile changed drastically during the period of the constant current discharge for 2 μs, when low transmission levels were maintained. No reflection of laser beam by the plasma column was observed even with the maximum sensitivity of the calory meter 3 which was smaller than 0.1 mJ, 1/200 of the incident laser energy. This is very important characteristics of the air discharge plasma shutter of this type, because the inter-cavity lasing can not be induced by these plasma columns when they are placed in a high power CO_2 laser amplifier chain.

In conclusion, an air discharge plasma shutter at the focal point of a CO_2 laser beam highly attenuated the transmission of it with a rise-time of less than 50 ns which was fast enough to cut off the retro-pulse in a high power laser system with long optical path. The low level transmission of 2∼3 % continued for more than 2 μs. During this time the back reflection from the plasma column into the focusing corn was extremely low. These characteristics of the plasma column obtained by discharge in atmospheric air are suitable for the application to a uni-directional guiding component in a high power CO_2 laser system.

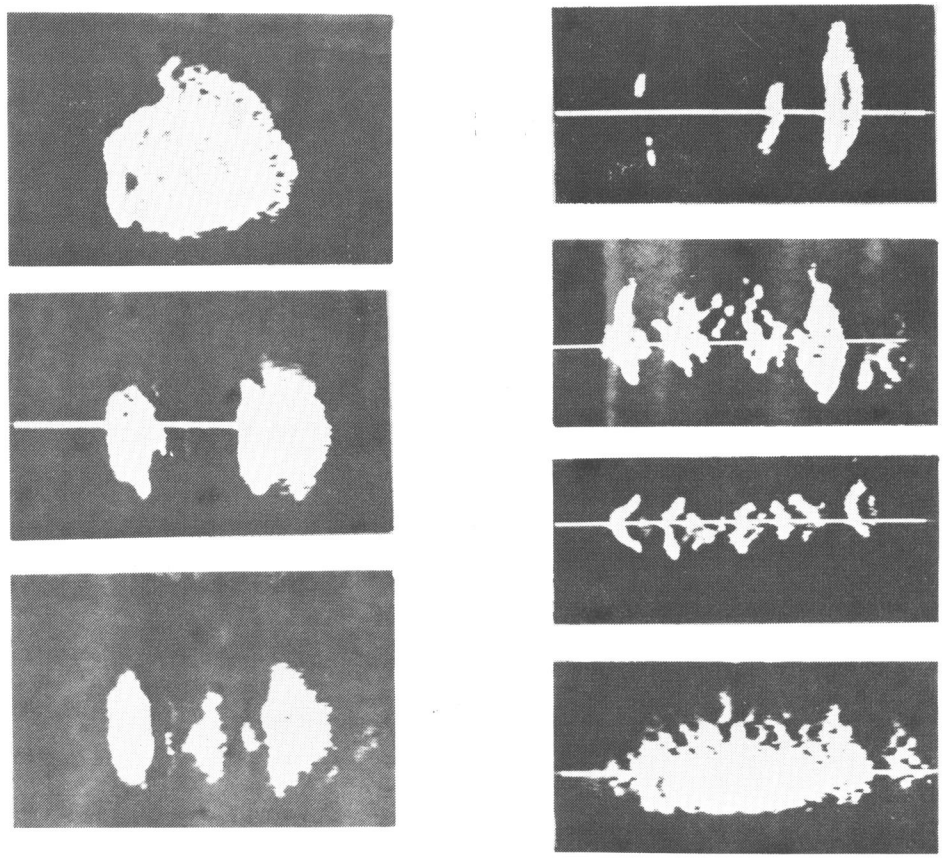

Fig.5-9. Magnified shadow graphs of the plasma column for various delay times. (A), (B), (C), (D), (E), (F), and (G) correspond to the delay times of 0 μs, 0.05 μs, 0.25 μs, 0.35 μs, 0.45 μs, 0.75 μs, and 1.2 μs after the start of the discharge respectively. (H) shows the experimental arrangement for the magnified shadow graphs.

5.4 Laser-induced plasma shutter

The plastic thin film plasma shutter and the air discharge plasma shutter can not be used in the high power stage, such as the exit of the final amplifier of a high power laser amplifier chain, because the air break down is induced by the outgoing laser beam. To be free from this breakdown, a laser induced-plasma shutter which could operate in vacuum was developed and its characteristics were investigated. One of this type was reported by Benjamin et al.[6], where a circular aperture of aluminum was set at the beam waist and the periphery of the beam hit the edge of the aperture and produced plasma. The stopping power of this plasma was tested by using an Ar ion laser as a probe. Here, we report the characteristics of a vacuum plasma shutter using the blow-off plasma produced by a laser beam on a plane target in a vacuum cell.

The experimental arrangement is shown in Fig.5-10. A flat carbon block was used as a target for a plasma source. A plasma-production laser beam which was split from the main beam by a beam splitter 1 was focussed onto the target perpendicular to the axis of the main laser beam. It was optically delayed with respect to the plasma-production laser beam. This plasma refracts the main laser beam or reflects it, if the density is larger than the critical density for 10.4 μm light ($10^{19}/cm^3$). Changing the position of the mirror 1, the optical delay (interval from the arrival of the plasma-production laser beam to that of the main laser beam at the focal point) could be set from 0 to 8.4 ns, which corresponds to the 2.5 m optical path

length difference. The focal point of a Ge lens 1 (f=100 mm) was placed on the carbon block. The focal point of a Ge lens 2 (f=140 mm) was placed on the axis of the plasma-production laser beam. The focal spot size of the Ge lens 2 was $\sim$ 0.6 mm, which was measured by a heat sensitive film placed at the focal point. The energies of the laser beams were monitored by the calory meters 1, 2, and 3. The temporal pulse shape of the transmitted main laser beam was measured by a Tektronix 7904 oscilloscope and a photon drag detector placed on the axis of the main laser beam. The energy of the laser beam was 0.5$\sim$1.5 J and the pulse width was 3 ns in the FWHM.

Fig.5-11 shows the transmission of the main laser beam through the laser induced plasma shutter as a function of the optical delay time, when the distance between the carbon block and the axis of the main laser beam was$\sim$0.8 mm, the plasma production laser energy was 100 mJ and the main laser energy was 250 mJ. The transmission decreased, as the optical delay increased. It is seen in Fig.5-11 that the minimum transmission was not reached within 8.4 ns. The transmission was then measured as a function of the distance between the carbon block and the axis of the main laser beam (D) for a fixed optical delay of 8.4 ns (see Fig.5-12). The energy of the main laser beam, the energy of the plasma production laser beam, and the pulse duration were 1.0$\sim$1.2 J, 0.4$\sim$0.5 J, and 3 ns (FWHM) respectively. A portion of the main laser beam was intercepted by the carbon block for D $\lesssim$ 0.3 mm, therefore the points plotted in Fig.5-12 represent the relative transmission with the plasma-production laser

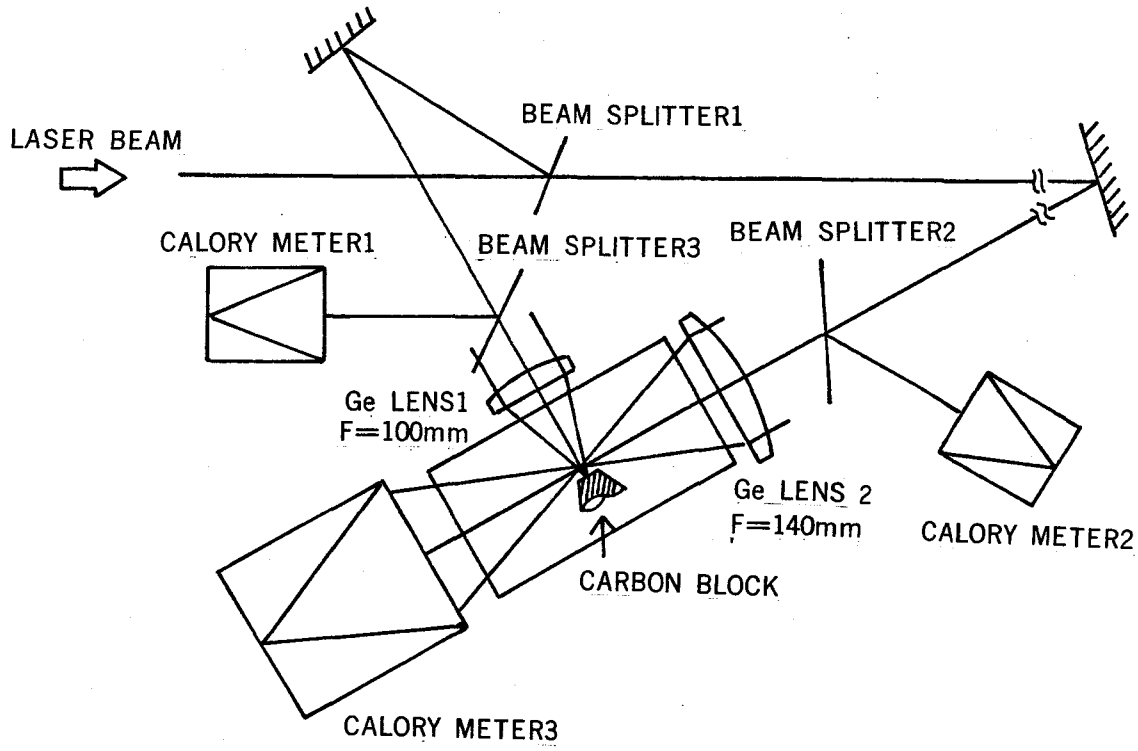

Fig.5-10. Experimental apparatus of the laser induced plasma shutter.

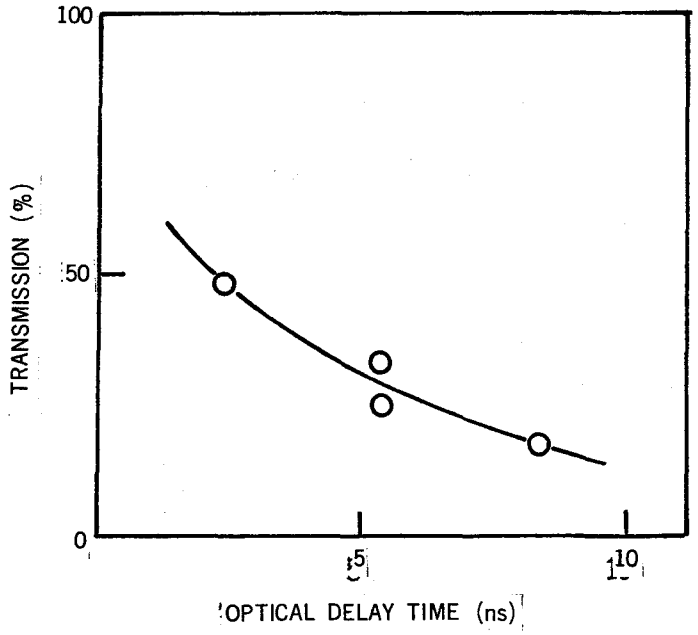

Fig.5-11. Transmission of the laser induced plasma shutter as a function of the optical delay time (interval between the arrival of the plasma production laser beam and that of the main laser beam on the focal point)

on and off. The minimum transmission with these conditions was 1/20 for D = 0.2 mm. The blow-off velocity of the edge of the laser induced plasma can thus be roughly estimated to be 2×10^6 cm/s.

To see the mechanism of the attenuation by the laser-induced plasma, the pulse shapes of the transmitted main laser beam and the input main laser beam were compared (see Fig.5-13). The pulse shape of the transmitted main laser beam was not changed, though the peak value became 1/20 of the input main laser beam. These were measured by the photon drag detector placed on the exit of the vacuum cell, and the diameter of it was approximately 1/10 of that of the main laser beam at that point, so the pulse shape showed the local transmission of the focal point. If the critical surface of the blow-off plasma for the 10.4 μm light had cut the main laser beam down at a certain time, the pluse shape of the transmitted main laser beam would have been disturbed. It can thus be said that the density of the blow-off plasma where it intercepted the main laser beam did not exceed critical density.

The attenuation characteristics through long time range were measured by using a cw CO_2 laser and a Cu-Ge detector. The experimental apparatus is shown in Fig.5-14. The cw CO_2 laser was used as a probe beam and was focussed in a vacuum cell. The focal spot size of $\sim$1 mm was measured by a heat sensitive film placed on the focal spot. A high power CO_2 laser pulse was focussed by a Ge lens (F=125 mm) on a carbon block placed beside the focal spot of the cw CO_2 laser beam which was focussed by a concave mirror (F=600 mm).

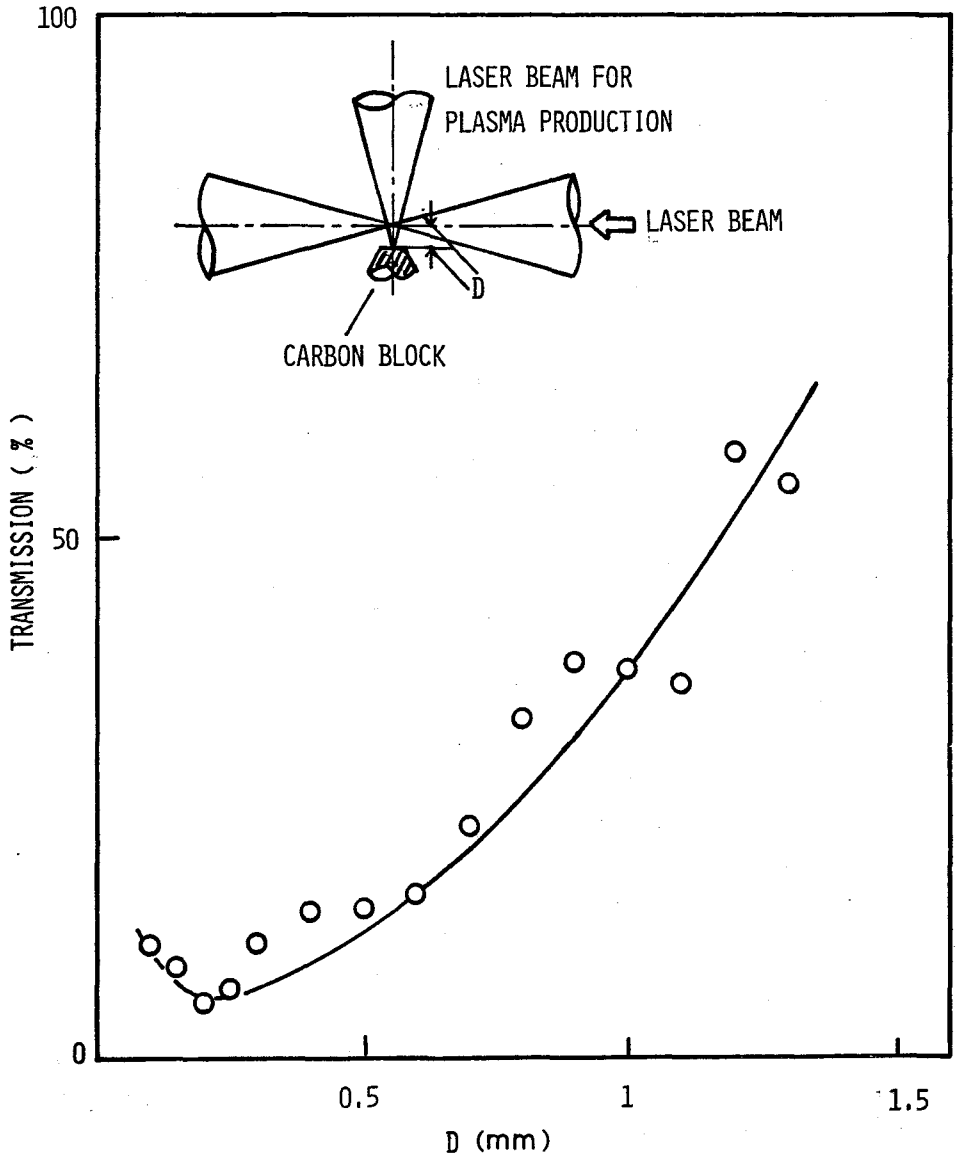

Fig.5-12. Transmission of the laser induced plasma shutter as a function of the distance between the carbon block and the axis of the main laser beam (D).

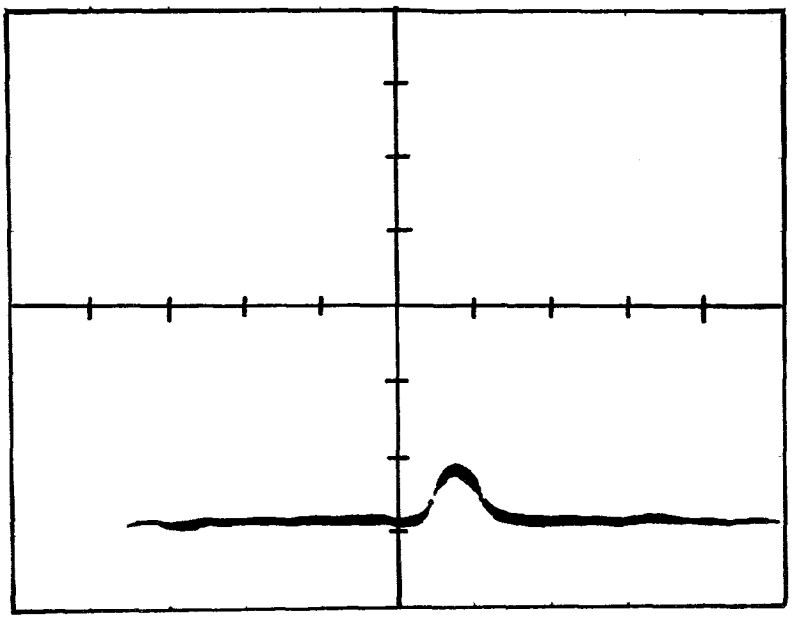

(a)

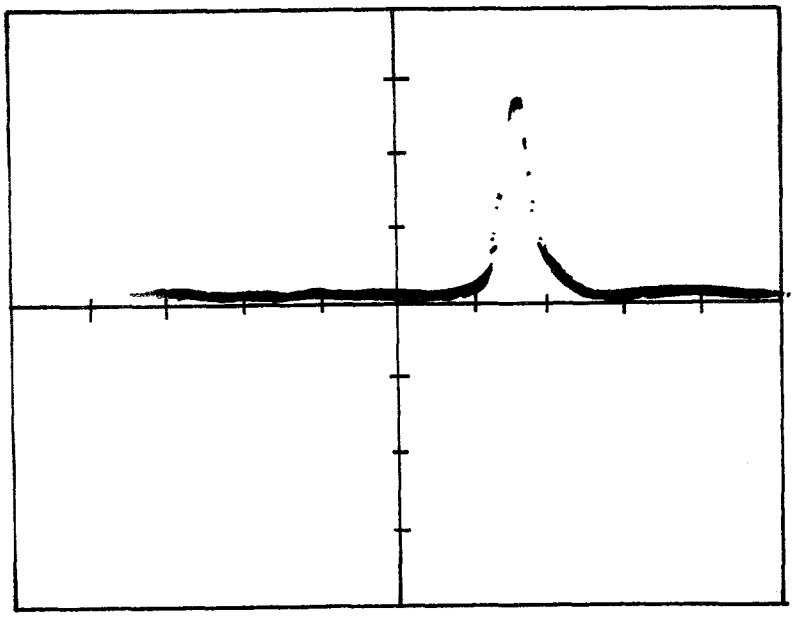

(b)

Fig.5-13. (a): The waveform of the transmitted main laser beam. (horizontal scale: 5 ns/div, vertical scale: 5 mV/div). (b): The waveform of the input main laser beam. (horizontal scale: 5 ns/div, vertical scale: 20 mV/div).

The experimental results are shown in Fig.5-15 (a), ~ (f). The distance between the carbon block and the axis of the probe laser beam (D) was chosen as a parameter. Fig.5-15 (b) shows a typical double-peak waveform. The first peak with a fast rise and the second peak with a slow rise are considered to correspond to the attenuation by a blow-off carbon plasma and a vaporized carbon respectively. As can be seen in this figure, the attenuation caused by a blow-off plasma does not continue long. The time required for reaching the minimum transmission is shown in Fig.5-16 as a function of the distance between the carbon block and the axis of the probe laser beam. The reciprocal of the slope of this curve, $\sim 3.9 \times 10^6$ cm/s, shows the blow-off velocity of the plasma. The risetime of the attenuation is shown in Fig.5-17. It increases roughly proportionally to D which is roughly proportinal to the blow-off time of the plasma. The increase of the risetime of the attenuation is considered to be caused by the decrease of the density gradient of the front of the blow-off plasma expanding into vacuum.

In conclusion, the blow-off plasma produced by a laser beam whose density was less than the critical density for 10.4 μm laser light could attenuate high power short pulse CO_2 laser beams (~ 1 J, 3 ns pulse width in the FWHM) in vacuum. The maximum attenuation ratio of 1/20 was obtained by using relatively low energy short laser pulse (~ 500 mJ, 3 ns in the FWHM). The attenuation region of the laser plasma shutter reaches up to 5.5 mm from the plasma source (carbon block). The time required for reaching the minimum

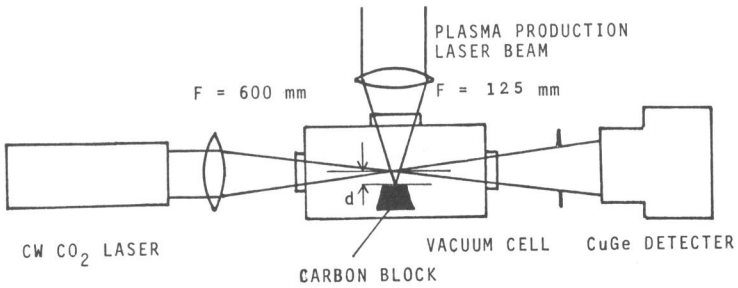

Fig.5-14. Experimental apparatus of the laser induced plasma shutter for measuring the attenuation characteristics through long time range.

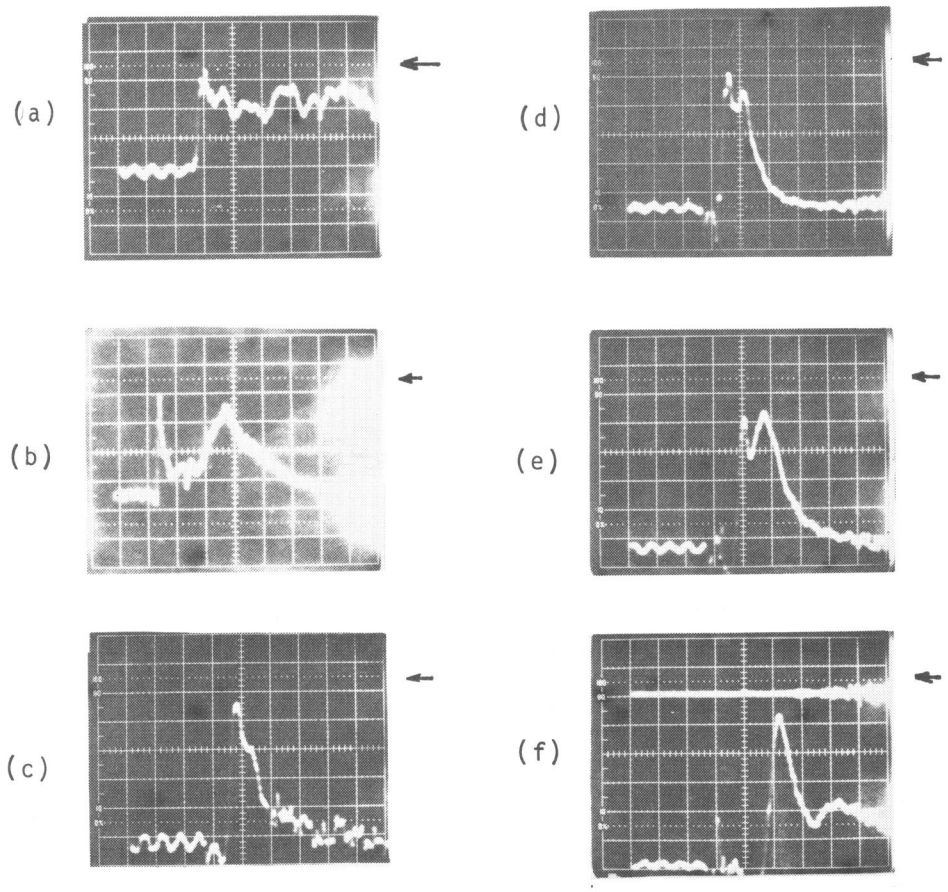

Fig.5-15. Transmission of a cw CO_2 laser beam through the laser induced plasma shutter. (a), (b), (c), (d), (e), and (f) represent the transmission of a cw CO_2 laser for D = 0.5 mm, 1.5 mm, 2.5 mm, 3.5 mm, 4.5 mm, and 5.5 mm respectively. (horizontal scale: 50 ns/div. Zero levels are indicated by arrows.)

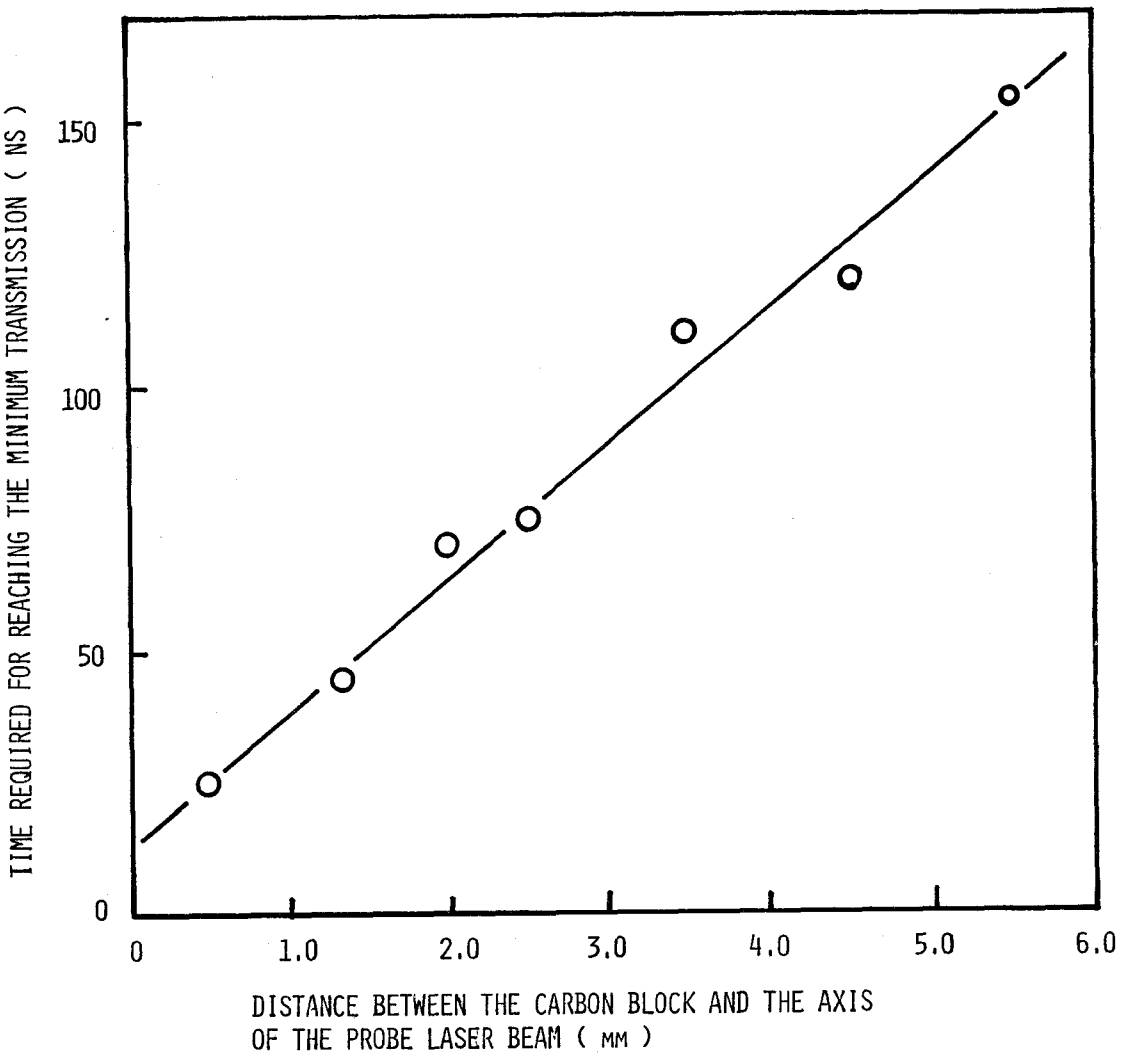

Fig.5-16. Time required to be the minimum transmission for the laser induced plasma shutter as a function of the distance between the carbon block and the axis of the probe laser beem.

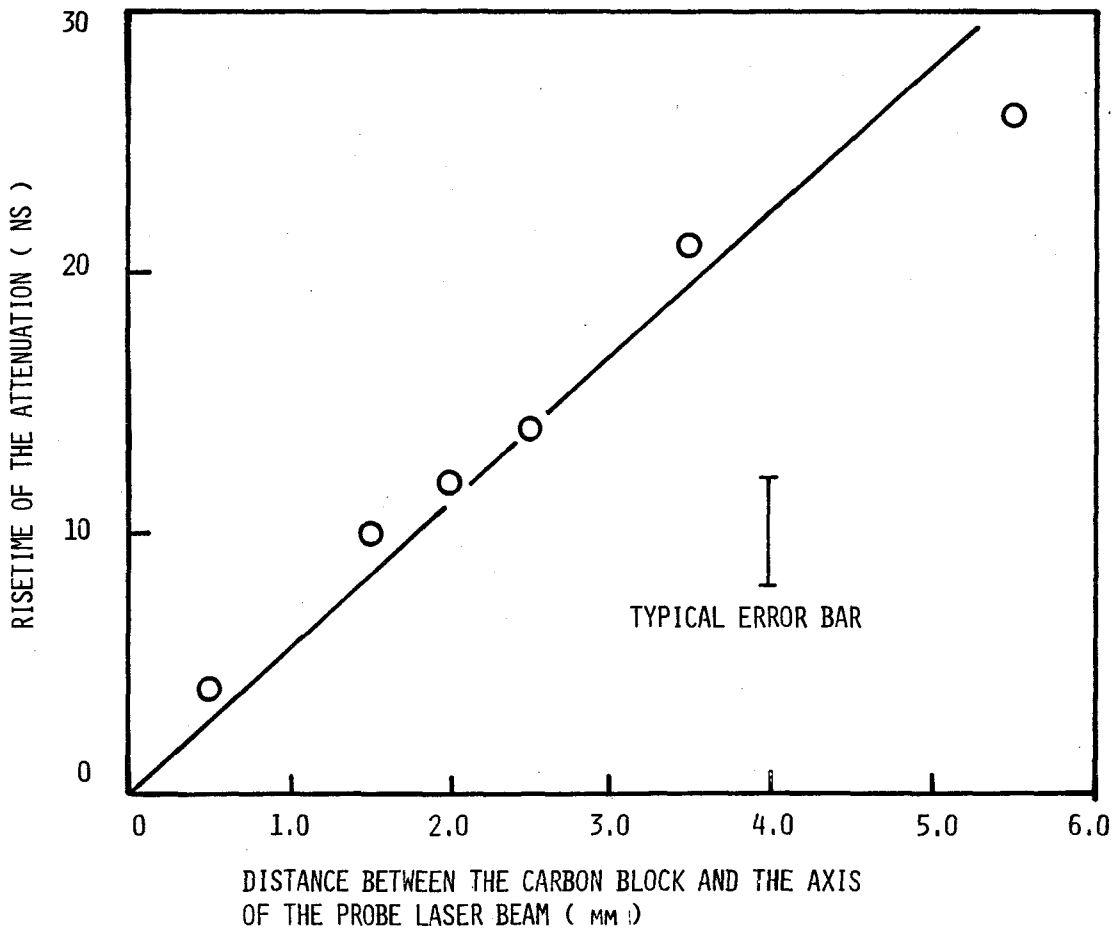

Fig.5-17. Risetime of the attenuation of the laser induced plasma shutter as a function of the distance between the carbon block and the axis of the probe laser beam.

transmission and the risetime of the attenuation were roughly proportional to the distance between the carbon block and the axis of the probe laser beam.

5.5 Summary

Three types of plasma shutters have been developed and the characteristics have also been investigated. These are a plastic thin film shutter, an air discharge plasma shutter, and a laser-induced plasma shutter. Their typical characteristics are summarized in Table 5-1. By using these plasma shutter suitably in a high power CO_2 laser amplifier chain, the retro-pulses from a target can be cut off fully enough not to cause optical damages on the laser devices. For further studies, attenuation characteristics of the laser induced plasma shutter in the higher input power region should be investigated, which could not be examined in this study.

Referances

1). C.R. Phipps, Jr., S.J. Thomas, and B. Lax, Appl. Phys. Lett. 25, 313 (1974).

2). C. Yamanaka, T. Yamanaka, T. Sasaki, K. Yoshida, M. Waki, and H.B. Kang, Phys. Rev. A6, 2335 (1972).

3). N.H. Burnett and M.C. Richardson, Rev. Sci. Instrum. 47, 241 (1976).

4). P. Weiss, Appl. Phys. Lett. 30, 261 (1977).

5). S. Ishii and B. Ahlborn, Rev. Sci. Instrum., 46, 1287 (1975).

6). R.F. Benjamin, D.B. Henderson, K.B. Mitchell, M.A. Stroscio,

		Thin film plasma shutter	Air discharge plasma shutter	Laser induced plasma shutter
Type of the operation		passive	active	active
Jitter of the operation		0	~10 ns	0
Attenuation ratio	for high power (>1J)	~1/20	~1/50	~1/20
	for low power (≤0.1J)	~1	~1/50	~1/20
Suitable operation stage in the amplifier chain		Exit of the oscillator (< 0.01J)	Exit of the pre-amplifier (1J~0.01J)	Exit of the main-amplifier (> 1J)
Operation condition		Both in vacuum and in air	in air only	in vacuum
Life time of the device		1 shot	infinite	Several hundreds shots (Limited by the lifetime of the carbon block)
Series operation for increasing the attenuation ratio		Not effective (Because of the power dependence)	effective	effective

Table 5-1. Typical characteristics of three types of plasma shutter

and J.Thomas, Appl. Phys. Lett. 31, 511 (1977)

Chapter 6 Summary

Conclusions of each chapter are summarized as follows

(Chapter 2)

In this chapter characteristics of multiline oscillation using inter-cavity etalon were described for gain-Q-switching oscillations and acousto-optic modelock oscillations. Multiline oscillation characteristics for modelock oscillations were explained perfectly by using the total cavity gain including both the loss of the inter-cavity etalon and the gain of the active medium, as well as for gain-Q-switching oscillations. It was shown that stable modelock multiline oscillations could be obtained for long time. It was shown that subnanosecond pulses could be obtained for an acousto-optic modelocking of a TEA CO_2 laser.

(Chapter 3)

It was shown that injection line forcing effect had the threshold power of an injecting cw laser, which varied according to the small signal gain of lines and detuning of the longitudinal-mode between the TEA CO_2 laser and the cw CO_2 laser. The thresholds of the injection line forcing effect were measured for the P(16) line of the 10.4 μm band as a function of the detuning angle, and it was confirmed that the angular range where the threshold value decreased was $\lesssim 0.35\pi$. For the angular region of $\gtrsim 0.35\pi$, the thresholds maintained the constant value of 100 mW.

(Chapter 4)

Increase in the energy extraction was demonstrated by using nine-line amplification of 3 ns pulses. Increase in the effective saturation energy by going to double-band amplification was shown comparing double-band two-line amplification with single-band two-line amplification. This increase was suppressed by the Fermi resonance between the lower (100) and (020) levels, and the amount of suppression was explained quantitatively. Saturation characteristics of 1 ns multiline pulses through a He-free electron beam controlled CO_2 laser amplifier were measured to obtain realistic data for constructing a high power CO_2 laser system. Large effective saturation energy was obtained even for single-line amplification of the P(20) line. This exceeded the theoretical value calculated by using the cross section of stimulated emission.

(Chapter 5)

Three types of plasma shutters have been developed and the characteristics have also been investigated. These are a plastic thin film shutter, an air discharge plasma shutter, and a laser-induced plasma shutter. Their typical characteristics are summarized in Table 5-1. By using these plasma shutter suitably in a high power CO_2 laser amplifier chain, the retro-pulses from a target can be cut off fully enough not to cause optical damages on the laser devices. For further studies, attenuation characteristics of the laser induced plasma shutter in the higher input power region should be investigated, which could not be examined in this study.

In conclusion, some of the difficulties in constructing a high power CO_2 laser amplification system were solved through this study. The prospect of its construction was demonstrated.

Acknowledgements

The author expresses his thanks to the late Prof. T. Murasaki, Prof. C. Yamanaka, and Prof. S. Nakai for their stimulations and guidances. He wishes to thank Prof. T. Sueta, Prof. T. Hirose, Prof. K. Imaich, Prof. T. Hayashi, Prof. T. Yoshikawa, prof. H. Fukuoka, Prof. T. Kakutani, Prof. A. Yamamoto, Prof. R. Koterazawa and Prof. S. Arimoto for their stimulations and encouragements. He wishes to thank Prof. K. Kasuya, and Dr. M. Matoba for their stimulations and useful discussions. Finally, he is especially greatful to Drs. H. Fujita, H. Nishimura, H. Daido, T. Takeda, K. Okamura, M. Sakajiri, F. Fukumaru, M. Inoue, K. Miyazato and K. Sawai for their hopeful discussions and continuing technical supports.

List of publications

1) "Improvement in energy extraction by a multiline/double band CO_2 laser", Y. Kawamura, H. Takeda, H. Fujita, M. Matoba, S. Nakai, and C. Yamanaka, Appl. Phys. Lett. 32, 722 (1978).

2) "Laser plasma isolator for a retropulse in a CO_2 laser amplifier chain", Y. Kawamura, H. Takeda, M. Matoba, S. Nakai, and C. Yamanaka, Appl. Phys. Lett. 33, 870 (1978)

3) "Attenuation characteristics of a high power CO_2 laser by an air discharge plasma column", Y. Kawamura, M. Matoba, S. Nakai , and C. Yamanaka, J. Appl. Phys. 50, 6159 (1979).

4) "Stable subnanosecond modelock multiline TEA CO_2 laser controlled by a NaCl etalon", Y. Kawamura, M. Sakajiri, M. Matoba, S. Nakai, and C. Yamanaka, Opt. Comm. 31, 178 (1979)

5) "Developement of a stable CO_2 modelock multiline oscillator" Y. Kawamura, M. Matoba, S. Nakai, and C. Yamanaka, The Transactions of The Institute of Electrical Engineers of Japan, 99-C, 251 (1979).